Chemical Thermodynamics and Thermal Analysis 12 (2023) 100120

Contents lists available at ScienceDirect

Chemical Thermodynamics and Thermal Analysis

journal homepage: www.elsevier.com/locate/ctta

Thermochemical models and data of layered double hydroxides, a review

Hanno Muire [a,c,*], Johan H. Zietsman [b,c], Frederick J.W.J. Labuschagné [a]

[a] Department of Chemical Engineering, University of Pretoria, Lynnwood Rd, Hatfield, Pretoria, 0002, Gauteng, South Africa
[b] Department of Materials Science and Metallurgical Engineering, University of Pretoria, Lynnwood Rd, Hatfield, Pretoria, 0002, Gauteng, South Africa
[c] Ex Mente Technologies, 447 Monica Rd, Lynnwood, Pretoria, 0081, Gauteng, South Africa

ARTICLE INFO

Keywords:
Layered double hydroxides
Thermochemistry
Modelling methods
Measurement techniques
Standard thermodynamic formation property data

ABSTRACT

Applications and reports of unique properties displayed by layered double hydroxides (LDHs) are steadily increasing. Fundamental insight into LDH synthesis is essential to developing sustainable production processes, and this can be acquired through an improved understanding of their underlying thermochemistry. The collection of work presented introduces LDHs, describes essential terminology, and provides a review of currently available literature focused on modelling methods and measurement techniques used to describe and capture standard thermodynamic formation property data of LDHs. A table of standard thermodynamic formation property data of LDHs is also presented at the end of the review.

1. Introduction

Research on Layered Double Hydroxides (LDHs) is becoming vast and expanding into many sectors of industry. LDHs are implemented for use as solid-base catalysts in applications such as hydrocarbon steam reforming, polymerisation of alkene oxides and alcohol synthesis. In the medical industry, LDHs are becoming prominent for applications as antacids, phosphate binders and drug delivery methods [1]. Another important industry use for LDHs is as additives for polymers in which these materials act as UV and thermal stabilisers, flame retardants and reinforcements for improvement on mechanical properties [2,1]. The environmental applications are numerous with uses such as pollutant adsorbers, decontaminants and environmental catalysts [3,1]. Novel applications for LDHs are also emerging where these materials can be used to substitute dye-sensitised materials in solar cells for energy production [4].

To drive the continued development of new applications and variations of LDHs a thorough understanding of LDH synthesis and thermochemical stability is required. This can only effectively be accomplished through Standard Thermodynamic Formation Property (STFP) data and modelling the expected synthesis reactions. The work presented here is a review of all available literature on the thermodynamic models and measurement methods used to acquire the STFP data for LDHs. Additionally, information regarding terminology and synthesis methods of LDHs is provided for background and understanding of the reviewed literature. All available STFP data on LDHs has been tabulated for easy reference and can be viewed in the final section of the review.

2. Layered double hydroxides

Information on chemical composition, terminology, synthesis methods and nomenclature used to describe LDHs is given in the section to follow. It is important to have a basic understanding of LDHs before moving to the thermodynamic models.

Hydrotalcite, a naturally occurring LDH, has the chemical formula $Mg_6Al_2(OH)_{16}CO_3.4H_2O$ and is regarded as the representative compound for the LDH class of compounds [5]. It consists of a brucite-like structure where some of the Mg^{2+} cations in brucite ($Mg(OH)_2$) are isomorphically substituted with Al^{3+}. The substitution induces a positive charge on the brucite-like layer. Anions such as carbonate (CO_3^{2-}) are intercalated between the brucite-like layers to maintain electroneutrality [1].

Hydrotalcite and many other anionic clays of this class are expressed with the general formula $[M^{2+}_{1-x}M^{3+}_x(OH)_2](A^{q-})_{x/q}.nH_2O$. The brucite-like layers, Fig. 1, are expressed with $[M^{2+}_{1-x}M^{3+}_x(OH)_2]$ and consists of divalent, M^{2+}, and trivalent, M^{3+}, metal cations bound with hydroxyl groups. The interlayer anion is represented by $(A^{q-})_{x/q}$ with q the associated charge. A stoichiometric relationship between the cations of the brucite-like layer and the anion of the interlayer is represented with x being the molar fraction of the trivalent cations to total metal cations [1]. The n water molecules at the end of the formula represent

* Corresponding author at: Department of Chemical Engineering, University of Pretoria, Lynnwood Rd, Hatfield, Pretoria, 0002, Gauteng, South Africa.
E-mail address: hanno.muire@tuks.co.za (H. Muire).

https://doi.org/10.1016/j.ctta.2023.100120
Received 25 July 2023; Received in revised form 21 September 2023; Accepted 26 September 2023
Available online 2 October 2023

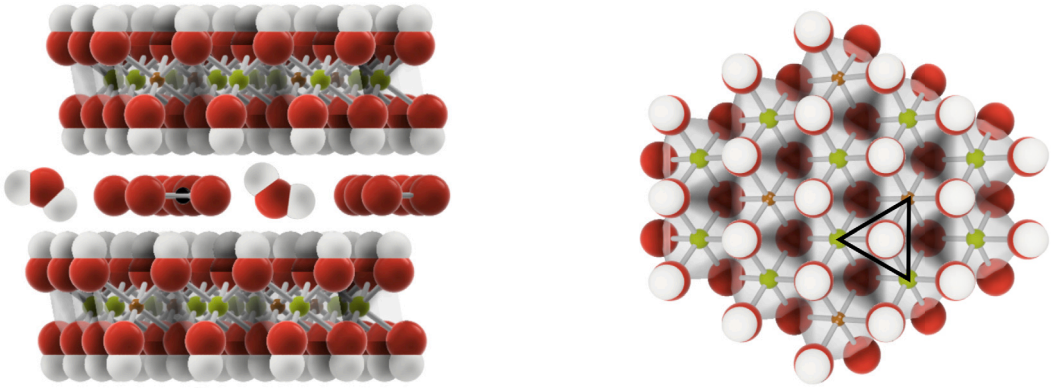

(a) Side view. (b) Top view.

Fig. 1. 3D Structure of a layered double hydroxid (green = Mg, brown = Al, red = O, white = H and black = C) [9]

Table 1
Cationic radii successfully used to synthesise LDH [10].

M^{+}	Radius (Å)	M^{2+}	Radius (Å)	M^{3+}	Radius (Å)	M^{4+}	Radius (Å)
Li	0.76	Fe	0.61	Al	0.54	V	0.58
Na	1.02	Co	0.65	Co	0.55	Ti	0.61
		Ni	0.69	Fe	0.55	Sn	0.69
		Mg	0.72	Mn	0.58	Zr	0.72
		Cu	0.73	Ga	0.62		
		Zn	0.74	Rh	0.6		
		Mn	0.83	Ru	0.68		
		Pd	0.86	Cr	0.69		
		Ti	0.86	V	0.74		
		Cd	0.95	In	0.80		
		Ca	1.00	Y	0.90		
		La	1.03				

weakly bound, adsorbed water on the surface of the brucite-like layer, water molecules strongly bound to the interlayer anion (crystal water) and excess water within the interlayer [6,7]. Crystal water is the crystallographically required quantity of water for the interlayer of an LDH and the desire is to analyse LDHs containing only this ideal amount of water for an associated interlayer anion but in most cases is unrealistic as LDHs are sensitive to humidity and can have stacking defects leading to a greater incorporation of excess water [6,8,7].

LDHs are referred to as clay materials as they share similar physical and chemical properties to clays. They have similar layered structures, a wide range of chemical compositions due to variable isomorphic substitution, variable layer charge densities, ion-exchange properties, reactive interlayer space, swelling in water, and rheological and colloidal properties [1].

The M^{2+} cationic radius is important for the formation of an LDH since the layered structure is not stable when this radius is < 0.6 Å [1]. Table 1 lists cations that have been successfully incorporated into the brucite-like layer. The majority of successfully synthesised LDHs incorporate combinations of divalent and trivalent cations, but combinations of monovalent and tetravalent cations with divalent and trivalent cations have also shown success [10].

Hydrocalumite, another natural occurring LDH, has Ca^{2+} instead of Mg^{2+} for the M^{2+} cation and Al^{3+} for M^{3+}. The Ca^{2+} cation has one of the largest radii, listed in Table 1, and results in a large difference, 0.46 Å, relative to Al^{3+}. This leads to a strong distortion of the local Ca^{2+} environment from a regular octahedron to a heptavalent crystal coordinate structure and enables the ordering of the divalent and trivalent cations into a corrugated brucite-like layer. Hydrocalumite has a fixed M^{2+} : M^{3+} ratio of 2:1 compared to hydrotalcite has a variable M^{2+} : M^{3+} ratio of between 1:1 and 3:1 [1].

A wide range of anions can also exist within the interlayer of an LDH. Some of the common anions are listed below in order of increasing selectivity [10]. The selectivity refers to a greater probability towards being intercalated into the interlayer with it being influenced by charge, charge density and hydrogen bonding [1].

$$NO_3^- < Br^- < Cl^- < F^- < OH^- < MoO_4^{2-} < SO_4^{2-} < CrO_4^{2-}$$

$$< HAsO_4^{2-} < HPO_4^{2-} < \text{Naphthol Yellow}^{2-} < CO_3^{2-}$$

The existence of multi- divalent and trivalent cations in single brucite-like layers has also been proven to be successfully synthesised. LDHs such as hydrotalcite and hydrocalumite can be seen as binary LDHs, consisting of only two metal cations. An LDH consisting of three metal cations can be labelled as a ternary LDH [11]. The existence of quaternary LDHs has also been demonstrated [1].

LDHs can be synthesised through various methods and are extensively discussed in literature [1,10,12]. The methods include co-precipitation, urea hydrolysis, induced hydrolysis, reconstruction, the sol-gel technique, and hydrothermal and anion exchange. More environmentally conscious methods are also emerging that utilise the mechanisms of dissolution-precipitation of solids to successfully synthesise LDHs. Forms of hydrotalcite and hydrocalumite have been synthesised through this method [13,14].

Several parameters that affect LDH synthesis are listed in Table 2.

Table 2
Parameters affecting synthesis.

Parameter	Ref	Parameter	Ref
pH	[15]	Reaction time	[14]
Solubility	[16]	Reactants' morphology	[14]
Temperature	[14]	Cation molar ratios	[17]
Pressure	[18]	Water to solid ratio	[14]
Aging period	[17]	Open/closed environment	[19]
Concentration of reactants	[16]	Mixing speed	[14]

Table 3
LDH group classifications [5].

Group Name	M^{2+} : M^{3+}	Interlayer spacing (Å)	Additional notes Brucite-like sheet constituents	Interlayer constituents
Hydrotalcite	3 : 1 favoured	7.8		CO_3^{2-}, Cl^-, OH^- or H_2O.
Quintinite	2 : 1 favoured	7.8		CO_3^{2-}, Cl^- or H_2O.
Fougerite	variable range	7.8	Fe^{2+} and Fe^{3+} predominantly, may contain some O^{2-} instead of OH^-.	
Woodwardite	variable range	8.9	M^{2+} = Ni^{2+}, Cu^{2+} and Zn^{2+}	SO_4^{2-} and H_2O
Cualstibite	variable range	9.7	M^{2+} = Cu^{2+}, Ni^{2+} or Zn^{2+} and M^{3+} = Al^{3+} or Fe^{3+}	$Sb(OH)6^-$
Glaucocerinite	variable range	11		SO_4^{2-} and H_2O
Wermlandite	variable range	11		SO_4^{2-}, H_2O and $B(H_2O)_6$ groups with B = Na^+, Ca^{2+}, Sr^{2+}, or similar large cations.
Hydrocalumite	2:1	11>	$(Ca,Al)(OH)_2$ corrugated brucite-like sheets. Ca^{2+} coordinated to a seventh ligand of interlayer water	May contain CO_3^{2-}, Cl^-, OH^-, SO_4^{2-} or H_2O.

Up until this point the words LDH, hydrotalcite and hydrocalumite have been used informally to provide background. However, proper definitions and nomenclature need to be provided to be accurate in using the correct terms, eliminate confusion and follow a set standard throughout. Nomenclature standards have been developed by Mills et al. [20,5] to help standardise naming and identification conventions for LDHs.

LDHs are seen as a class of anionic clay compounds, natural and synthetic, consisting of a layered structure that is derived from brucite ($Mg(OH)_2$). Hydrotalcite ($Mg_6Al_2(OH)_{16}CO_3 \cdot 4H_2O$) is the original model mineral for the supergroup of minerals it represents and consists of eight defined groups. The group nomenclature for LDHs, Table 3, follows a set of guidelines by the Commission on New Minerals, Nomenclature and Classification (CNMNC) that are based on mineral grouping conventions of crystal structure and chemical composition [20,5]. The CNMNC developed these guidelines to help standardise the introduction of new minerals and mineral names and to rationalise mineral nomenclature. The guidelines for LDHs are considered as hybrid as groups are first defined by interlayer spacing and secondly by the M^{2+} : M^{3+} ratios in the brucite layers. Polytype and polytypoids are not regarded as separate species and, like topologically similar polymorphs, distinguish is made by the addition of a crystallographic suffix to the mineral name [5]. Tables in the referenced literature further list the names and formulae for different minerals found in the groups [5].

The nomenclature for synthetic LDH phases proposed by Mills et al. [5] provides information about the chemistry, crystallography of the phase and uses the following formula: LDH, $yM^{2+}zM^{3+} \cdot A[B] - C$, to identify it as a synthetic compound. The proportions of M^{2+} and M^{3+} are indicated by the molar amounts y and z. A, represents the intercalated anion, B is an interlayer cation; and C is the polytype symbol. This nomenclature system beneficially conveys the M^{2+} : M^{3+} ratio that leads to quantitative constraints on the interlayer anion content and the creation of an empirical formula, with $\pm$ H_2O in the interlayer, to be written [5]. It captures important data for describing the chemical properties of synthetic LDH phases, however, it is unfortunately not adequate for this review of the literature.

In sections to follow, the thermochemistry of both synthetic LDHs and LDHs estimated from simpler constituent compounds are discussed, and it is important to indicate the correct amount of interlayer anions and water as STFP data vary with composition. Therefore, synthetic and estimated LDHs are reported only with their full compositional formula. Additionally, to provide a form of structured categorising between different LDHs, in Table 7, mineral group names are provided even though reported LDHs is either synthetic or estimated. The LDH group classifications by Mills et al. [5] will help evaluate many more LDHs and will hopefully continue to evolve to accommodate the growing number of novel LDHs being synthesised.

3. Thermodynamic modelling methods

This section presents modelling methods to estimate STFP data. Some of these methods are regarded as more general and can be applied to various classes of compounds. However, for the review, these general methods are described in context to LDHs. The methods employ the use of simpler constituent compounds that have structures similar to the target compound to describe its STFP data. Modelling methods specific to LDHs are also described for determining STFP data. Application of these methods with their strengths and weaknesses towards modelling LDHs are discussed.

The reviewed literature consists of concepts that are alike or have a common relationship with a mathematical or chemical expression but with differing notations. To maintain brevity it was decided to disregard any old notation and to follow, as best possible, a uniform set of notation based on current International Union of Pure and Applied Chemistry (IUPAC) standards [21]. However, one adjustment was made to the notation used for reporting on the STFP data. The subscript area used for indicating the temperature at 298 K was re-purposed, Equation (1), to indicate the compound name associated with the thermodynamic property. Therefore, temperature is not indicated in the subscript of the thermodynamic property anymore and all mentioned equations and thermodynamic properties should be regarded as being at standard state conditions. The standard state conditions for the investigated compounds are defined as 298 K and 1 bar.

$$\Delta_f \tilde{G}^\circ_{298}(\text{Compound name, func}) = \Delta_f \tilde{G}^\circ_{\text{Compound name}}(\text{func}) \quad (1)$$

The modelling methods are classified as either Complete Solid Phase (CSP) models that factor in interlayer water, or Partial Solid Phase (PSP) models that disregard interlayer water. With slight modification, some of the PSP models, discussed, can be adapted into CSP models. For CSP, the basic additive methods and mechanical mixture models, are first described followed by Volume-Based Thermodynamics (VBT) and the Thermodynamic Difference Rules (TDR), solubility methods, the three-term approximation method and lastly hydration modelling. The PSP models consist of the redox potential method, additional mixture models and solid-solution models. All the models reported, in the two sections, are implicitly ranked from the more simplistic additive methods followed by more complex methods for estimating STFP data of LDHs.

Information for more clarity regarding the specific terms, quantities, symbols and units used in the review can be found in the respective nomenclature and abbreviation sections at the end of the review.

3.1. Complete solid phase models

The principal method to obtain a value, for a desired property, of a more complex, target compound is by stoichiometrically adding values together of constituent compounds to represent it. This seems

simple but is based on certain assumptions, to be discussed, and if not aware can be completely inaccurate. Therefore, it may apply to certain compounds but not to others and requires experimental data for confirmation.

3.1.1. Additive methods

The first mathematical relationship, introduced by Helgeson et al. [22] as an additivity method, is to estimate the standard entropy of a solid by assuming a reference reaction, Equation (3), that involves reactants and products that are structurally analogous to each other with known entropies. It importantly has a net zero entropy of reaction, $\Delta_r \bar{S}^\circ = 0$ [22]. It is also applied to reactions involving hydrated solids where it is necessary to determine the associated standard entropy of the bound water. The concept of "net zero" is also applicable for the volume of reaction, $\Delta_r \bar{V}^\circ = 0$ and heat capacity of reaction, $\Delta_r \bar{C}_p^\circ = 0$, and is a popular model used in many cement publications [23–26]. It originates from the basic additivity relation of Equation (2) where the standard molar entropy ($\bar{S}_j^\circ$) of the target compound (j), is determined by the sum of the standard molar entropy of the constituent compounds ($\bar{S}_i^\circ$), such as an oxide or hydroxide, multiplied by the respective stoichiometric coefficients (ν_i) of the constituent compounds within the target compound [22].

$$\bar{S}_j^\circ = \sum_{i=1}^{n} \nu_i \bar{S}_i^\circ \tag{2}$$

The incorporation of reaction equation(s) changes Equation (2) into Equation (3) to factor in the stoichiometric reaction coefficients. The stoichiometric coefficients of the i^{th} compound ($\hat{\nu}_{i,r}$) and the $\hat{i}^{th}$ target compound ($\hat{\nu}_{\hat{i},r}$) in the r^{th} reference reaction are positive for products and negative for reactants. This can be similarly expressed for $\Delta_r \bar{C}_p^\circ$, including heat capacity coefficients (a_0, a_1, a_2, a_3), and $\Delta_r \bar{V}^\circ$.

$$\bar{S}_{\hat{i}}^\circ = \sum_{i=1}^{\hat{i}-1} \hat{\nu}_{i,r} \bar{S}_i^\circ / \hat{\nu}_{\hat{i},r} \tag{3}$$

An adaptation to Equation (2) is Equation (4) with the molar volume of the target compound, ($\bar{V}_j$) and the molar volume of the i^{th} constituent compound within the target compound are factored in with a constant, k' [27].

$$\bar{S}_j^\circ - k'\bar{V}_j = \sum_{i=1}^{x} \nu_i (\bar{S}_i^\circ - k'\bar{V}_i) \tag{4}$$

The absolute entropy ($\bar{S}^\circ$) of a compound is related to its heat capacity, $\bar{C}_V^\circ$ or $\bar{C}_p^\circ$, and factors such as temperature, volume and pressure that affect $\bar{S}^\circ$ will also affect the heat capacity with a significant effect at temperatures near 298.15 K [28]. Smaller errors are yielded with Equation (4) than Equation (2) as it can account for such factors including the combined effects of volume, coordination state and magnetic order-disorder transformation which specifically occurs in minerals with transition metals. It can be corrected by applying different $\bar{S}^\circ - k'\bar{V}$ for different coordination states, which can allow for the correction of the magnetic disorder. The absence of this from Equation (2) becomes evident when different polymorphs of the same composition are to be analysed. Identical $\bar{S}^\circ$ values are produced with Equation (2) for different polymorphs because their selected oxide or hydroxide constituents are the same. However, this should not be possible for two or more polymorphs, with the same chemical composition, to have the same $\bar{S}^\circ$ as different structures have different heat capacities and therefore different entropies. Therefore, Equation (2) and Equation (4), are not as straightforward to use and require careful consideration in the selection of the constituent oxides or hydroxides [28].

The method of Helgeson et al. [22] was used to estimate heat capacity coefficients (a_0, a_1, a_2, a_3) for LDHs found in cement phases. It was employed together with the three-term approximation method, to be discussed, to eventually estimate $\bar{S}^\circ$, $\Delta_f \bar{H}^\circ$ and $\Delta_f \bar{G}^\circ$ for the phases.

These equations used to model $\bar{S}^\circ$ has the drawback of errors that can arise and propagate if the entropies of the reference compounds are already inaccurate, or if the compounds are not selected carefully [22]. This is also applicable to the additive methods of the mechanical mixture models that are discussed next. This is an important factor for hydrates, as the binding state of water, such as adsorbed water or structurally bound crystal water and excess water, has a significant influence on the entropy estimations [28].

3.1.2. Mechanical mixture model

The mechanical mixture model is analogous to the additive methods described in the previous section. In its application, it uses STFP data for LDHs determined experimentally on specific LDH compositions and existing STFP data of constituent compounds with more simplistic chemical compositions to calculate enthalpies, entropies and Gibbs free energies of reactions [29–33].

The first proposed chemical reaction, Equation (5), consists of constituent compounds of a metal hydroxide, $M(OH)_2$ with a brucite structure, $Al(OH)_3$ with a gibbsite structure, and MCO_3 with a calcite structure. The second chemical reaction, Equation (6), consists of a metal oxide, MO with a periclase structure and Al_2O_3 with a corundum structure for solid constituent compounds. The CO_2 and H_2O are in the gas and liquid phase.

$$(1-3x/2)M(OH)_2(s) + x/2MCO_3(s) + xAl(OH)_3(s) + nH_2O(l) \longleftrightarrow M_{1-x}Al_x(OH)_2(CO_3)_{x/2} \cdot nH_2O(s) \tag{5}$$

$$(1-x)MO(s) + x/2Al_2O_3(s) + x/2CO_2(g) + (1+n)H_2O(l) \longleftrightarrow M_{1-x}Al_x(OH)_2(CO_3)_{x/2} \cdot nH_2O(s) \tag{6}$$

The enthalpies are called the enthalpy of formation for single-cation compounds from hydroxides, carbonates and water ($\Delta_f \bar{H}_{scc}$), Equation (7), and the enthalpy of formation from oxides ($\Delta_f \bar{H}_{ox}$), Equation (8). Both enthalpies describe a difference between the $\Delta_f \bar{H}^\circ_{LDH}$ of the target compound, the LDH, and the simpler constituent compounds of which it may be composed. Particulars of how experimentally determined $\Delta_f \bar{H}^\circ_{LDH}$ are obtained are explained in the Thermodynamic Data Measurement Techniques section 4.

$$\Delta_f \bar{H}_{scc} = \Delta_f \bar{H}^\circ_{LDH} - (x/2\Delta_f \bar{H}^\circ_{MCO_3} + x\Delta_f \bar{H}^\circ_{Al(OH)_3} + (1-3/2x)\Delta_f \bar{H}^\circ_{M(OH)_2} + n\Delta_f \bar{H}^\circ_{H_2O}) \tag{7}$$

$$\Delta_f \bar{H}_{ox} = \Delta_f \bar{H}^\circ_{LDH} - ((1-x)\Delta_f \bar{H}^\circ_{MO} + x/2\Delta_f \bar{H}^\circ_{Al_2O_3} + x/2\Delta_f \bar{H}^\circ_{CO_2} + (1+n)\Delta_f \bar{H}^\circ_{H_2O}) \tag{8}$$

Allada [29] reported that two of three CoAl LDHs investigated had $\Delta_f \bar{H}_{scc}$ that ranged between $0-10\ KJ\,mol^{-1}$. These small values lead to the proposal that STFP data can be estimated by treating LDHs as a mixture of structurally similar binary compounds. The greater a $\Delta_f \bar{H}_{scc}$ value deviates from zero (ideally, $\Delta_f \bar{H}_{scc} = 0$, $\Delta_f \bar{H}_{ox} = 0$), the less reliable the mechanical mixture model becomes. This was subsequently demonstrated by LDH phases bearing Ni,Zn and Mg that produced $\Delta_f \bar{H}_{scc}$ ranging in $10-20\ KJ\,mol^{-1}$ [30].

The mechanical mixture model should be regarded as an additivity model for estimating $\Delta_f \bar{H}^\circ_{298}$ and $\Delta_f \bar{G}^\circ_{298}$ for LDHs. It encompasses the same additivity concepts used in the model of Helgeson et al. [22] for describing $\Delta_r \bar{S}^\circ, \Delta_r \bar{C}_p^\circ$ and $\Delta_r \bar{V}^\circ$ but now specifically for $\Delta_f \bar{H}_{scc}$ applied to LDHs [22]. The mechanical mixture model is even described as an additivity conjecture and later published literature describes that the previously mentioned LDHs approximately fit the model [31,34]. Therefore, to consolidate like concepts, $\Delta_f \bar{H}_{scc}$, can be rewritten as the enthalpy of reaction between single-cation constituent compounds and an LDH at standard state conditions, $\Delta_r \bar{H}^\circ_{scc} = \Delta_f \bar{H}_{scc} = 0$. The same applies for $\Delta_f \bar{H}_{ox}$ that can be seen as the enthalpy of reaction between oxides and an LDH at standard state conditions, $\Delta_r \bar{H}^\circ_{ox} = \Delta_f \bar{H}_{ox} = 0$.

The intended use of the mechanical mixture model is to be able to estimate $\Delta_f \bar{H}^\circ_{LDH}$ from a weighted sum of constituent compounds, Equation (9). The calculations involving $\Delta_r \bar{H}^\circ_{scc}$ and $\Delta_r \bar{H}^\circ_{ox}$ serve to experimentally prove that the assumption of using a mechanical mixture model is valid. Similarly utilising certain additional thermodynamic assumptions and equations, to be discussed, $\Delta_f \bar{G}^\circ_{LDH}$ using Equation (10), can also be proven.

$$\Delta_f \bar{H}^\circ_{LDH} = \frac{x}{2}\Delta_f \bar{H}^\circ_{MCO_3} + x\Delta_f \bar{H}^\circ_{Al(OH)_3} + \left(1 - \frac{3}{2}x\right)\Delta_f \bar{H}^\circ_{M(OH)_3} + n\Delta_f \bar{H}^\circ_{H_2O} \quad (9)$$

$$\Delta_f \bar{G}^\circ_{LDH} = \frac{x}{2}\Delta_f \bar{G}^\circ_{MCO_3} + x\Delta_f \bar{G}^\circ_{Al(OH)_3} + \left(1 - \frac{3}{2}x\right)\Delta_f \bar{G}^\circ_{M(OH)_3} + n\Delta_f \bar{G}^\circ_{H_2O} \quad (10)$$

An initial assumption of the mechanical mixture model was by assuming that the crystal structures of the hydroxide and carbonate constituent compounds are similar to that of an LDH. Each constituent compound can have multiple different structural forms each with unique STFP data. The assumption is rationalised with the cation and anion coordination environments in the hydrotalcite being structurally similar, and therefore energetically similar, to the hydroxide and carbonate constituent compounds [29]. The binary hydroxides and carbonates have layered structures and ideally react to form a new ternary layered material, an LDH, in which cations are located in a layer similar to that of their binary precursors, with anions found above or below these planes. Thus, the reactants, the hydroxide and carbonate constituent compounds, and the products, LDHs, are structurally similar.

More recently published STFP data for LDHs (containing Mg, Zn, Zr, Al, Fe and Li) do not mention or validate the mechanical mixture model [8,35–37,34]. For some of these published compositions, the $\Delta_f \bar{H}_{scc}$ and $\Delta_f \bar{H}_{ox}$ data deviate far greater from zero than the initial LDH data produced by Allada [29] revealing that the model may be less reliable for some compositions and that the assumption of similar crystal structures must be applied cautiously.

As for $\Delta_r \bar{H}^\circ_{scc}$, the entropy contribution ($\Delta_r \bar{S}^\circ_{scc}$), Equation (11), can be calculated and be used to calculate the Gibbs free energy of single-cation compounds ($\Delta_r \bar{G}^\circ_{scc}$) with Equation (12).

$$\Delta_r \bar{S}^\circ_{scc} = \bar{S}^\circ_{LDH} - \left(\frac{x}{2}\bar{S}^\circ_{MCO_3} + x\bar{S}^\circ_{Al(OH)_3} + (1 - 3/2x)\bar{S}^\circ_{M(OH)_2} + n\bar{S}^\circ_{H_2O}\right) \quad (11)$$

It first requires that $\bar{S}^\circ_{LDH}$ to be calculated. If no electronic or magnetic effects are considered, $\bar{S}^\circ_{LDH}$ is determined form vibrational (S_{vib}) and configurational (S_{config}) entropies with Equation (13).

$$\Delta_r \bar{G}^\circ_{scc} = \Delta_r \bar{H}^\circ_{scc} - T\Delta_r \bar{S}^\circ_{scc} \quad (12)$$

$$\bar{S}^\circ_{LDH} = S_{vib} + S_{config} \quad (13)$$

The S_{vib} is calculated using $\bar{C}_p$ data, Equation (14), determined experimentally using relaxation calorimetry (discussed in the Thermodynamic Data Measurement Techniques section 4) [38,37,34].

$$S_{vib} = \int_0^T \frac{\bar{C}_p}{T}\, dT \quad (14)$$

The maximum entropy contribution from the mixing of species is done by calculating S_{config}. It arises from the disordered arrangement of cations, vacancies, anions and water within the LDH structure [37]. A two-sublattice model was initially implemented for the LDH, $Mg_{0.74}Al_{0.26}(OH)_2(CO_3)_{0.13}\cdot 0.39H_2O$, with Mg^{2+} and Al^{3+} cations mixing randomly within the brucite layer, and CO_3^{2-}, H_2O, and any vacant sites mix randomly within the interlayer. The model was later implemented in other LDH studies with progressive improvements to the thermodynamic description of LDH structures [39,37,34]. However, to keep the explanation simple the original model implementation is discussed here.

The configurational entropy, S_{config}, Equation (15), is the sum of the individual terms, $S_{config,brucite}$, for the brucite layer and $S_{config,interlayer}$ for the interlayer.

$$S_{config} = S_{config,brucite} + S_{config,interlayer} \quad (15)$$

The calculation for the number of vacant sites, n_{Va}, within the interlayer is first done by considering the number of possible sites for water, $n_{modelled}$ [40]. This is shown by Equation (16) where N_{anion} is the number of sites occupied by the anions, $N_{anion} = 3$ for CO_3^{2-} having 3 oxygen sites, x is the cation mole fraction, and q is the charge of the anion.

$$n_{modelled} = 1 - N_{anion}\frac{x}{q} \quad (16)$$

The vacant sites, n_{Va}, are then calculated with Equation (17).

$$n_{Va} = n_{modelled} - n \quad (17)$$

This results in $n_{modelled} = 0.61$ and $n_{Va} = 0.22$ moles of vacant sites for the mentioned LDH.

Using the base of 1 mole LDH results in, $n_t = 0.74$, for the total moles of the mixing species, CO_3^{2-}, H_2O and vacant sites, in the interlayer ($0.13 + 0.39 + 0.22 = 0.74$). The interlayer fractions are then, $x_a = 0.522$, for the mole fraction of CO_3^{2-}, $x_w = 0.301$, the mole fraction of water and x_{Va} =0.177 for the mole fraction of vacant sites. The $S_{config,interlayer}$ contribution is then calculated with Equation (18) with R being the universal gas constant of 8.314 J mol^{-1} K.

$$S_{config,interlayer} = -Rn_t(x_a \ln x_a + x_w \ln x_w + x_{Va}\ln x_{Va}) \quad (18)$$

With the assumption of cations mixing randomly within the brucite layer, Equation (19), (with $x = 0.26$) is applied to calculate the contribution of $S_{config,brucite}$.

$$S_{config,brucite} = -R[(1-x)\ln(1-x) + x\ln x] \quad (19)$$

The resulting S_{config}, Equation (15), from the original study was 10.95 J mol^{-1} K^{-1} and combining it with the S_{vib} of 85.58 J mol^{-1} K^{-1}, Equation (13), and using Equation (11) results in a near zero, 1.40 kJ mol^{-1}, $T\Delta_r \bar{S}^\circ_{scc}$ contribution at 298 K.

Using Equation (12) with the calculated $\Delta_r \bar{H}^\circ_{scc}$ and $T\Delta_r \bar{S}^\circ_{scc}$ terms results in a $\Delta_r \bar{G}^\circ_{scc}$ that can be used to calculate $\Delta_f \bar{G}^\circ_{LDH}$ with Equation (20).

$$\Delta_f \bar{G}^\circ_{LDH} = \Delta_r \bar{G}^\circ_{scc} + \left(\frac{x}{2}\Delta_f \bar{G}^\circ_{MCO_3} + x\Delta_f \bar{G}^\circ_{Al(OH)_3} + (1 - 3/2x)\Delta_f \bar{G}^\circ_{M(OH)_2} + n\Delta_f \bar{G}^\circ_{H_2O}\right) \quad (20)$$

The reported $\Delta_f \bar{G}^\circ_{LDH}$ value for $Mg_{0.74}Al_{0.26}(OH)_2(CO_3)_{0.13}\cdot 0.39H_2O$, found in Table 7, was -1043.08 ± 2.07 kJ mol^{-1}. It has to be mentioned that this reported $\Delta_f \bar{G}^\circ_{LDH}$ excludes the small S_{config} contribution contradictorily included in the described calculation of $\Delta_r \bar{G}^\circ_{scc}$. Allada [31] originally reasoned that the contributions to $\bar{S}^\circ_{LDH}$ from cation mixing in the LDH brucite layer are smaller than the maximum random mixing of $S_{config,brucite}$. The substitution of Al^{3+} for M^{2+} results in a +1 charge, increasing the probability for substitution centres to be as far apart as possible. The contribution from mixing in the interlayer between water and carbonate would also be reduced from the maximum random mixing of $S_{config,interlayer}$ because of charge balance and bonding considerations. Factoring in all of these considerations, the actual contribution of S_{config} to calculating $\Delta_f \bar{G}^\circ_{LDH}$ would be significantly less than the maximum and S_{config} would not outweigh S_{vib} [31]. Subsequent studies have however included the S_{config} contribution in their calculations for calculating $\bar{S}^\circ_{LDH}$ [39,37,34].

3.1.3. Volume-Based Thermodynamics (VBT)

The VBT and TDR models can determine full sets of STFP data for ionic materials [41]. The models describe solid and liquid salts and in-

clude the solid hydrate (e.g. $AlCl_3 \cdot 6H_2O$) and solvate (e.g. $AlCl_3 \cdot SO_2$, $AlCl_3 \cdot H_2S$, or $AlCl_3 \cdot 7\,NH_3$) members. The models are mathematically simple and only require minimal skill in the use of spreadsheets to compute values [41].

The "volume-based" part in the name of the method, "Volume-Based Thermodynamics", refers to the use of the formula unit volume (V_N) as the basis for calculation [42]. The formula unit (N) is an integer representing the number of molecules (formula units) contained within a crystallographic unit cell and V_N, Equation (21), can be calculated directly from the unit cell volume (V_{cell}).

$$V_N = \frac{V_{cell}}{N} \tag{21}$$

The "Thermodynamics" part of the name refers to the discovery of linear correlations between entropies and volumes, between enthalpies of formation and volumes, and between lattice energies and volumes. It is reported that entropies of many classes of condensed phases, both organic and inorganic, are closely linearly proportional to V_N. The thermoelastic property of compressibility for solids has been demonstrated as being dependent on V_N [43,44]. Correlations of V_N with physical properties of liquids such as viscosity, density, electrical conductivity, melting point and critical micelle concentrations of ionic liquids and other ionic surfactants have also been demonstrated [45,46].

The molar volume ($\bar{V}$) can also be used to calculate V_N, Equation (22), for various inorganic solids [28]. However, depending on the availability of material property data there are other approaches as well to calculate V_N and can be viewed at the reference [42].

$$V_N = \bar{V} \times 10^{21} / N_A \tag{22}$$

It is reported that the number of intermolecular interactions increases proportionally to V_N. Therefore, V_N acts to represent the extent of interaction, averaged over the set of interactions, even though it is largely independent of the interactions and leads to the understanding it is independent of the structure of liquids or crystals [42].

The VBT method was developed due to the lack of standard entropy data available for inorganic materials in standard thermochemical tables [47]. Experimental determination of $\bar{S}°$ by calorimetry methods can be a tedious and non-trivial process. These inconveniences in acquiring $\bar{S}°$ measurements have led to an increased dependence on modelling methods for thermochemical data [47].

The VBT method, Equation (23), shows that there is a direct relationship between, $\bar{S}°$, and V_N. The method was initially demonstrated with a range of stoichiometries for minerals that consisted of 65 anhydrous (M_bA_a) and 67 hydrated ionic solids ($M_bA_a \cdot nH_2O$) [47]. In a separate study, it was also demonstrated to be useful for organic liquids and solids [48].

$$\bar{S}° = kV_N + c \tag{23}$$

Regression analyses were performed on these datasets as well on an additional 99 anhydrous inorganic minerals. Equation (24) to Equation (26) were formulated, with associated errors (Table 4), to provide a means to estimate standard molar entropy for the specific group of materials [47].

$$\bar{S}° = 1360V_N + 15;\ \text{for anhydrous ionic solids} \tag{24}$$

$$\bar{S}° = 1579V_N + 6;\ \text{for hydrated ionic solids} \tag{25}$$

$$\bar{S}° = 1262V_N + 13;\ \text{for anhydrous minerals} \tag{26}$$

The errors, Table 4, has a minor effect on the calculation for change in molar Gibbs energy ($\Delta\bar{G}$), Equation (27) [47].

$$\Delta\bar{G} = \Delta\bar{H} - T\Delta\bar{S} \tag{27}$$

The change in molar enthalpy ($\Delta\bar{H}$) is most often reported with units of kJ mol^{-1} due to the size of the reported values whereas the change in molar entropy $\Delta\bar{S}$ is reported with general International System of Units (SI) units of J mol^{-1} K^{-1}. It indicates that $\Delta\bar{S}$ values are normally smaller by a factor of a thousand relative to $\Delta\bar{H}$ and results in the $\Delta\bar{G}$ also being reported with units of kJ mol^{-1}. This difference in the size of the values indicated by the units, for the quantities of $\Delta\bar{G}$, $\Delta\bar{H}$ relative to $\Delta\bar{S}$, allows for larger errors to be tolerated.

Table 4
Average percentage error of fitted plots for VBT equations to data points.

Equation	Error (%)
Equation (24)	11.5
Equation (25)	7.4
Equation (26)	12.6

3.1.4. Thermodynamic Difference Rules (TDR)

The TDR method uses the simple concept of a linear equation ($y = mx + c$) that is manipulated so that the left-hand side of the equation represents a difference, $y - c = mx$ [49].

The TDR method uses this base equation to describe the following set of equations termed "difference" functions. The equations involve a difference, linear, relationships between a thermodynamic property (P) of a hydrated salt, and its corresponding anhydrous salt. The difference function, Equation (28), is linearly dependent on the number of molecules of water of crystallization, n, contained in the hydrate. The constant ($\theta_P(H_2O, s\text{-}s)$), or slope of the linear equation, is in effect describing the change in P when a new water molecule is inserted into or removed from the crystal lattice. The "s-s" denotes that it is derived from the difference between solid-state parent and solid-state hydrate.

$$P(M_bA_a \cdot nH_2O, s) - P(M_bA_a, s) = n \cdot \theta_P(H_2O, s\text{-}s) \tag{28}$$

The difference function can also be written for a relationship, Equation (29), between hydrated salts of different hydration states.

$$P(M_b A_a . nH_2O, s) - P(M_b A_a, s) = (n - \acute{n}) \cdot \theta_P(H_2O, s\text{-}s) \tag{29}$$

The difference rule also applies to other solvates (SOL), besides hydrates, and values for the constants ($\theta_P(SOL, s\text{-}s)$) can be found in a table in the referenced literature [49]. If sufficient data is given to calculate $\theta_P(SOL, s\text{-}s)$ for a given solvate, then the corresponding thermodynamic property, P, of any parent or solvate, real or hypothetical, can be estimated, regardless of whether there was a previously known example of a solvate formed in the series [49]. The enthalpy of formation ($\Delta_f\bar{H}°$) for solvates not yet studied in the solid state can also be estimated ($\theta_{\Delta_f\bar{H}°}(SOL, s\text{-}s)$) based on liquid or even gas-state values of $\Delta_f\bar{H}°$. This should, in general, be applicable for all property constants $\theta_P(SOL, s\text{-}s)$ [49].

Implementation of the TDR and VBT methods depends on the unknown thermodynamic property desired for a specific compound (existing or theorised). The availability of already existing thermodynamic and physical property data on the compound or the chemical series of the compound will also help determine the route of calculation. The referenced literature on the TDR and VBT methods provide insight, examples, prescription diagrams and additional calculation methods, as to which calculation route would be the best to follow with limited physical property and thermodynamic data to determine the desired property value [50–52,41]. Additionally, a table of sources where TDR and VBT has directly been applied and should be viewed at the reference for further insight into applications for the methods [41].

The VBT and additivity method were the main forms of assessment for the reliability of standard entropies compiled in two major datasets [22,28]. These datasets, *Cemdata* and *Thermoddem*, consist of cement phases, some of which are LDHs [26,53,28]. The authors revealed that the additivity method is sensitive to the selection of the constituent compounds when estimating $\bar{S}°$ for LDHs. The estimated $\bar{S}°$

values for LDH cement phases showed deviation from the established VBT linear trend line, Equation (25). Therefore, STFP values used for the constituent compounds require careful selection as their composition and structure will directly influence the final value of the target compound [28].

3.1.5. Solubility methods

The concentration of metal cations in an aqueous solution in equilibrium with an LDH phase can be calculated with the use of experimentally derived and estimated STFP data. The required $\Delta_f\bar{G}°$ values for pure LDH phases can be obtained experimentally through calorimetry methods, to be discussed, or estimated with a model such as the mechanical mixture model, Equation (10). The dissolution reaction equation of an LDH, Equation (30), can be written in terms of $\Delta_r\bar{G}°$, Equation (31), and be used to determine equilibrium solubility product (K_{sp}) values with Equation (32).

$$M^{2+}_{1-x}M^{3+}_{x}(OH)_2(CO_3)_{x/2}.nH_2O(s) + 2H^+(aq) \longleftrightarrow (1-x)M^{2+}(aq) + xM^{3+}(aq) + \frac{x}{2}CO_3^{2-}(aq) + (n+2)H_2O(l) \quad (30)$$

$$\Delta_r\bar{G}° = (1-x)\Delta_f\bar{G}°_{M^{2+}} + x\Delta_f\bar{G}°_{M^{3+}} + \frac{x}{2}\Delta_f\bar{G}°_{CO_3^{2-}} + (n+2)\Delta_f\bar{G}°_{H_2O} - 2\Delta_f\bar{G}°_{H^+} - \Delta_f\bar{G}°_{LDH} \quad (31)$$

$$\Delta_r\bar{G}°(T) = -RT\ln K_{sp}(T) \quad (32)$$

The dissolution reaction, Equation (30), if assumed ideal, can be represented with K_{sp} as Equation (33).

$$K_{sp}(T) = \frac{a^{(1-x)}_{M^{2+}}a^{x}_{M^{3+}}a^{x/2}_{CO_3^{2-}}}{a^{2}_{H^+}} = \frac{[M^{2+}]^{(1-x)}[M^{3+}]^{x}[CO_3^{2-}]^{x/2}}{[H^+]^2} \quad (33)$$

For non-ideal conditions in solution chemistry, Equation (33), can be altered to Equation (34) that requires the use of activity coefficients (γ_i) to describe the non-ideality.

$$K_{sp}(T) = \frac{\gamma_{M^{2+}}[M^{2+}]^{(1-x)}\gamma_{M^{3+}}[M^{3+}]^{x}\gamma_{CO_3^{2-}}[CO_3^{2-}]^{x/2}}{\gamma_{H^+}[H^+]^2} \quad (34)$$

The main factors of influence on K_{sp} are the solution chemistry, the concentration of species, ionic activities of considered species and temperature. Software such as MINTEQ or Gibbs Energy Minimisation Selektor (GEMS) can be used to aid in calculation and to estimate the concentrations of the desired species at equilibrium [33,26].

As described, the method above is a procedure to estimate the concentration of metal cations in an aqueous solution, in this case for LDHs, but it can also be performed in reverse to determine STFP data [54]. However, performing the method in reverse prevents the amount of interlayer water in the LDH from being factored in correctly into the calculation of K_{sp} as the solid LDH and liquid water are considered constant. The value for $\Delta_f\bar{G}°_{LDH}$ is also undetermined and only calculated at the end. The dissolution reaction, K_{sp} and $\Delta_r\bar{G}°$ are adapted to stoichiometrically balance out. Experimental equilibrium concentration data of an aqueous species in equilibrium with a solid is first obtained and with a dissolution reaction, Equation (35), K_{sp} is calculated, Equation (36), followed by the calculation of $\Delta_r\bar{G}°$ and finally $\Delta_f\bar{G}°_{LDH}$, Equation (32) and (37)

$$M^{2+}_{1-x}M^{3+}_{x}(OH)_2(CO_3)_{x/2}(s) \longleftrightarrow (1-x)M^{2+}(aq) + xM^{3+}(aq) + \frac{x}{2}CO_3^{2-}(aq) + (2)OH^-(aq) \quad (35)$$

$$K_{sp}(T) = [M^{2+}]^{(1-x)}[M^{3+}]^{x}[CO_3^{2-}]^{x/2}[OH^-]^2 \quad (36)$$

$$\Delta_r\bar{G}° = (1-x)\Delta_f\bar{G}°_{M^{2+}} + x\Delta_f\bar{G}°_{M^{3+}} + \frac{x}{2}\Delta_f\bar{G}°_{CO_3^{2-}} + 2\Delta_f\bar{G}°_{OH^-} - \Delta_f\bar{G}°_{LDH} \quad (37)$$

STFP data of some LDHs presented in Table 7 have been obtained through this process and unfortunately the amount of interlayer water present is either just disregarded or inferred without an analytical technique for conformation [54,55].

Other potential errors in data determined from solubility methods can arise from the reaction equation considered for the target compound. The reaction equation affects the solution concentrations and ionic activities [55].

The three-term approximation method, discussed next, is a specialised solubility-based method and an overview with additional concerns regarding solubility measurements are further elaborated on.

3.1.6. Three-term approximation method

Cement contains various phases of LDHs and within cement research, it is commonly modelled with the three-term approximation method. A large portion of the STFP data found in Table 7 consists of LDHs found in cement literature [26,53,23]. To experimentally derive $\bar{S}°$ of a compound the third law of thermodynamics has to be applied through the measuring of the isobaric heat capacity ($\bar{C}_p$) over a temperature range of near 0 K to above 298.15 K and applying Equation (14) (with $S_{vib} = \bar{S}°$) over the same temperatures. However, it is infrequently applied to derive $\bar{S}°$ for cement hydrates. The experimental setup required for the direct determination of $\bar{C}_p$ near absolute zero is not widely available, and it is difficult to prepare cement hydrates, target compounds, and their selected constituent compounds, in high enough purity to enable precise measurement of $\bar{S}°$ values [28].

The three-term approximation method has taken preference as its implementation avoids these issues. In short, it first uses experimentally measured solubility data, done at various temperatures, to calculate K_{sp} values for cement hydrates, such as LDHs. Fittings are then applied to the K_{sp} data by manipulating $\Delta_r\bar{S}°$, which leads to $\bar{S}°$, acquired from the so-called three-term approximation equations. The $\bar{S}°$ value that gives the best fit to the measured solubility data is regarded to be the one representing the desired cement hydrate [23]. A similar method of approximation is also employed by Blanc et al. [53] and is for self-review. A systematic description of the three-term approximation method's implementation is given as follows [23].

An initial step is to gather the necessary STFP data, of structurally similar, constituent compounds. Analogous to the already discussed models this is done as more complex compounds such as LDHs may need to be estimated with the use of this data if none are available. Formulation of reference reactions, such as Equation (38), is used to estimate $\bar{C}°_p$ or a_0, a_1, a_2, a_3 values with Equation (39) that do not involve "free" water. The only water considered is water bound to compounds involved in the reference reaction. This is to minimise errors associated with varying strengths of bonding for water and to effectively apply the additive method for, $\Delta_r\bar{C}°_p = 0$, which require these criteria [22].

$$Ca_4Al_2(CO_3)(OH)_{12}\cdot 5H_2O(s) + 0.5\,CaSO_4\cdot 2H_2O(s) + 0.5\,CaSO_4(s) \longleftrightarrow Ca_4Al_2(SO_4)(OH)_{12}\cdot 6H_2O(s) + CaCO_3(s) \quad (38)$$

$$\bar{C}°_p(T) = a_0 + a_1T + a_2T^{-2} + a_3T^{-0.5} \quad (39)$$

It is followed by the formulation of a separate dissolution reaction of the desired compound, such as Equation (40).

This together with standard, partial molal, thermodynamic properties of considered aqueous species, the extended Debye-Hückel, Equation (41), is applied to calculate the activity coefficients (γ_i) [23].

$$Ca_4Al_2(CO_3)(OH)_{12}\cdot 5H_2O(s) \longleftrightarrow 4Ca^{2+}(aq) + 2AlO_2^-(aq) + CO_3^{2-}(aq) + 4OH^-(aq) + 9H_2O(l) \quad (40)$$

$$\log\gamma_i = \frac{-Az_i^2\sqrt{I}}{1 + b\alpha_i\sqrt{I}} + bI \quad (41)$$

Temperature-dependent K_{sp} values, Equation (42), can be calculated from the γ_i according to the dissolution reactions and experimental solubility data (ion concentration data) measured at various temperatures. $\Delta_r\bar{G}°$ is calculated from Equation (32) with the K_{sp} values.

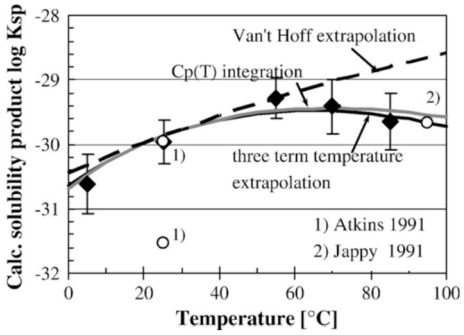

Fig. 2. Graphical representation of three-term approximation method applied to experimentally-derived solubility products for siliceous hydrogarnet [23].

$$K_{sp}(T) = \frac{\gamma_{Ca^{2+}}[Ca^{2+}]^4 \gamma_{AlO_2^-}[AlO_2^-]^2 \gamma_{CO_3^{2-}}[CO_3^{2-}]}{\gamma_{OH^-}[OH^-]^4} \tag{42}$$

The described equations to follow will eventually calculate $\bar{S}°$, $\Delta_f \bar{H}°$, $\Delta_f \bar{G}°$ of the STFP data for the target compound. The $\bar{C}_p°$ or a_0, a_1, a_2, a_3 values, as described previously, were determined with the additive method of Helgeson et al. [22].

The three-term approximation has a separate temperature-dependent $\log K_{sp}$ function, Equation (43), that depends on the relationships of Equation (44) to Equation (49). It is modelled by fitting it to calculated K_{sp} values obtained from experimentally measured solubility data at various temperatures [23]. The chosen value for $\Delta_r \bar{G}°$ used in the fitting is calculated from Equation (32) with a K_{sp} value at 298 K from the experimentally measured solubility data. This is done to stay at standard state conditions. $\Delta_r \bar{H}°$ or $\Delta_r \bar{S}°$ is then the only property that needs to be adjusted until the best fit, Fig. 2, between the $\log K_{sp}$ function and calculated K_{sp} at 298 K is achieved. The heat capacity of reaction, $\Delta_r \bar{C}_p°(T) = \Delta_r \bar{C}_p°(T_0) = \Delta a_0$, is assumed to be constant over the temperature range of 273 – 373 K.

$$\log K_{sp}(T) = A_o + A_2 T^{-1} + A_3 \ln T \tag{43}$$

$$A_0 = \frac{0.4343}{R}.[\Delta_r \bar{S}°(T_0) - \Delta_r \bar{C}_p°(T_0)(1 + \ln T_0)] \tag{44}$$

$$A_2 = \frac{0.4343}{R}.(\Delta_r \bar{H}°(T_0) - \Delta_r \bar{C}_p°(T_0) \cdot T_0) \tag{45}$$

$$A_3 = \frac{0.4343}{R}.\Delta_r \bar{C}_p°(T_0) \tag{46}$$

$$\Delta_r \bar{S}°(T) = \Delta_r \bar{S}°(T_0) + \Delta_r \bar{C}_p°(T_0) \ln \frac{T}{T_0} \tag{47}$$

$$\Delta_r \bar{H}°(T) = \Delta_r \bar{H}°(T_0) + \Delta_r \bar{C}_p°(T_0)(T - T_0) \tag{48}$$

$$\Delta_r \bar{G}°(T) = \Delta_r \bar{H}°(T) - T\Delta_r \bar{S}°(T) \tag{49}$$

Depending on the chosen property, $\Delta_r \bar{S}°$ or $\Delta_r \bar{H}°$, for fitting, the other is calculated in the process with Equation (49) and together with the previously created dissolution reactions and standard, partial molal, thermodynamic properties of the aqueous species, the STFP data for the complex solid, the LDH, can finally be calculated. This is one variation of implementation and can differ depending on the available data of the target compound under investigation.

The three-term approximation method can be susceptible to producing inaccurate thermodynamic property data. Measured K_{sp} values can be incorrectly factored in by being missing, incorrect, subject to significant uncertainty, or failing to represent the hydrates studied. The possibility also exists, even with meticulous experimental control, that the calculated K_{sp} values can represent a condition in which the solution is not in equilibrium with respect to the hydrate, and is subjected to the effects of one or more remnant precursors and/or metastable phases [28].

The accuracy of entropy data obtained via this method is also rarely assessed using independent techniques, but exceptions do exist that use additional measurement techniques for confirmation [38,28]. Therefore, caution should be applied regarding the use of STFP data obtained via K_{sp} data and if possible it is ideal to verify modelled data with additional modelling and analytical techniques.

3.1.7. Hydration modelling

A multi-method approach was employed to determine the Standard Thermodynamic Reaction Property (STRP) data ($\Delta_r \bar{G}°, \Delta_r \bar{H}°, \Delta_r \bar{S}°$) for different hydration states of hydrocalumite grouped LDHs. The approach used a combination of X-Ray Diffraction (XRD), Thermogravimetric Analysis (TGA), sorption balance measurements, sorption calorimetry and the salt-hydrate pair-humidity buffer method to determine the data [56].

XRD and TGA were used to determine the $\bar{V}$ of the different hydration states under specific drying conditions influenced by temperature and Relative Humidity (RH). These analytical techniques cannot identify the exact value of RH at which an absorption/desorption process takes place. Therefore, supporting data was obtained by sorption balance, sorption calorimetry and the salt pair-humidity buffer method [7]. The sorption balance and sorption calorimetry are described in the Thermodynamic Data Measurement Techniques section 4.

The salt-hydrate pair-humidity buffer method was developed to determine the RH at which a change in hydration state occurs. It applies the salt-hydrate pair principle which considers a thermodynamic equilibrium between hydrate pairs. This is a system in equilibrium, Equation (50), consisting of two hydration states of the same salt, and the water vapour pressure of the surrounding gas [56].

$$MA \cdot n_1\, H_2O(s) \longleftrightarrow MA \cdot n_2\, H_2O(s) + (n_1 - n_2)H_2O(g) \tag{50}$$

$\Delta_r \bar{G}°$ is calculated with Equations (51), (52) and (53) by defining the activities of the pure solid phases as 1 with $RH = f/f^* \times 100$.

$$K_f = \frac{a_{MA.n_1H_2O} a_{H_2O}{}^{n_1 - n_2}}{a_{MA.n_2H_2O}} = f_{H_2O}^{n_1 - n_2} \tag{51}$$

$$\Delta_r \bar{G}°(T) = -RT \ln K_f(T) \tag{52}$$

$$\Delta_r \bar{G}°(T) = -RT \ln(f_{H_2O}^{n_1 - n_2}) = (n_2 - n_1)RT \ln(f_{H_2O}) = (n_2 - n_1)RT \ln \frac{f^*_{H_2O} RH}{100} \tag{53}$$

Finally, the van't Hoff equation, Equation (54), is used to calculate $\Delta_r \bar{H}°$ with K_f and $\Delta_r \bar{S}°$ is calculated with Equation (49).

$$\frac{\partial(\ln K)}{\partial(1/T)} = -\frac{\Delta_r \bar{H}°}{R} \tag{54}$$

The standard thermodynamic properties of reaction values only indicate a change in hydration state, between two states, but together with STFP data of LDHs from Table 7, the STFP data were modelled for new hydrocalumite grouped phases at different hydration states [7,23,57].

The calculations for the target compound's STFP data are simply done by rearranging of reaction equation to make desired STFP data of the target compound the subject. An example for $Ca_4Al_2(OH)_{12}CO_3 \cdot 3H_2O$ is given for the reaction, Equation (55), to calculate $\Delta_f \bar{H}°$ with Equation (56) and (57).

$$Ca_4Al_2(OH)_{12}CO_3 \cdot 3\,H_2O(s) + 2\,H_2O(g) \longleftrightarrow Ca_4Al_2(OH)_{12}CO_3 \cdot 5\,H_2O(s) \tag{55}$$

$$\Delta_r \bar{H}° = \Delta_f \bar{H}°_{Ca_4Al_2(OH)_{12}CO_3 \cdot 5H_2O} - \Delta_f \bar{H}°_{Ca_4Al_2(OH)_{12}CO_3 \cdot 3H_2O} - 2\Delta_f \bar{H}°_{H_2O} \tag{56}$$

$$\Delta_f \bar{H}°_{Ca_4Al_2(OH)_{12}CO_3 \cdot 3H_2O} = -\Delta_r \bar{H}° + \Delta_f \bar{H}°_{Ca_4Al_2(OH)_{12}CO_3 \cdot 5H_2O} - 2\Delta_f \bar{H}°_{H_2O} \tag{57}$$

STFP data for saturated vapour ($\Delta_f \bar{H}°_{H_2O} = -241.82$ kJ mol^{-1} at 298 K) was used for the specific mole amount of interlayer water. The

method, demonstrated by the example, to calculate $\Delta_r\bar{G}°, \Delta_r\bar{H}°$ and $\Delta_r\bar{S}°$ for the different hydration states, requires STFP data on already existing LDHs and cannot be employed without this data. $\Delta_r\bar{H}°$ can also be calculated with sorption calorimetry, discussed in the Thermodynamic Data Measurement Techniques section 4, with Equation (78) and (79).

3.2. Partial solid phase models

The models described in the section to follow ignore the associated n amount of water (adsorbed, crystal and excess water) with the general LDH composition being described as $[M^{2+}_{1-x}M^{3+}_x(OH)_2](A^{q-})_{x/q}$.

3.2.1. Redox potential method

This method uses redox potentials (potentiometry) to calculate $\Delta_f\bar{G}°$ values for some Green Rust (GR) type LDHs [58]. These LDHs have the general formula of $[Fe^{2+}_{1-x}Fe^{3+}_x(OH)_2][A^{q-}_{(x/q)}\cdot(n/q)H_2O]$ that can contain anions such as sulphate (SO_4^{2-}), carbonate (CO_3^{2-}) and chloride (Cl^-) [59,60]. In short, the data is estimated with the use of the Nernst equation, Equation (58), utilising recorded potentials from GR systems and an applicable equilibrium reaction.

$$E = E° + \frac{RT}{zF}\log Q \tag{58}$$

The example, Equation (59), provides a half-cell reaction on the formation of a GR LDH with sulphate (GR_{SO_4}) [58].

$$6\,Fe(OH_2)(s) + SO_4^{2-}(aq) \longleftrightarrow Fe^{2+}_4Fe^{3+}_2(OH)_{12}(SO_4)(s) \tag{59}$$

$\Delta_f\bar{G}°_{GR_{SO_4}}$ is calculated with the associated Nernst equation, Equation (60), and the standard redox potential ($E°$) of the system at equilibrium, Equation (61). The values for the redox potential (E) and the activity of SO_4^{2-} ($a_{SO_4^{2-}}$) are obtained from experimentation. The measured redox potentials must represent true equilibrium potentials.

$$E = E° + 0.0296\log a_{SO_4^{2-}} \tag{60}$$

$$E° = \frac{1}{2F}((\Delta_f\bar{G}°_{GR_{SO_4}} - \Delta_f\bar{G}°_{Fe(OH)_2} - \Delta_f\bar{G}°_{SO_4^{2-}}) \tag{61}$$

Unfortunately, the method does not factor in interlayer water and STFP data of recorded GR infer the amount of interlayer water with a crystallographic study or just exclude it [61,62,59,63–67].

3.2.2. Additional mixture models

The mechanical mixture model initially proposed by Allada [29] was further built upon with the creation of additional mixture models, and resulted in four models together with a fifth model, a general model, which is a combined average of all the models, to describe LDHs with structurally similar compounds [30,68].

Model 0, Equation (62), is a combination of the hydroxide compounds $M^{2+}(OH)_2$, $M^{3+}(OH)_3$ and an anion A^{q-}.

$$(1-x)M^{2+}(OH)_2(s) + (x)M^{3+}(OH)_3(s) + (x/q)A^{q-}(aq)$$
$$\longleftrightarrow [M^{2+}_{1-x}M^{3+}_x(OH)_2](A^{q-})_{(x/q)}(s) + xOH^-(aq) \tag{62}$$

Model 1, Equation (63), is a combination of the hydroxide compounds, $M^{2+}(OH)_2$ and $M^{3+}(OH)_3$, with a hydride anion, $H_q(A^{q-})$.

$$(1-x)M^{2+}(OH)_2(s) + (x)M^{3+}(OH)_3(s) + (x/q)H_qA^{q-}(aq)$$
$$\longleftrightarrow [M^{2+}_{1-x}M^{3+}_x(OH)_2](A^{q-})_{(x/q)}(s) + xH_2O(aq) \tag{63}$$

Model 2, Equation (64), is a combination of the hydroxide compounds, $M^{2+}(OH)_2$ and $M^{3+}(OH)_3$, with a divalent metal-anion complex, $M^{2+}(A^{q-})_{(2/q)}$. This model is similar to the mixture model proposed by Allada [29].

$$(1-3x/2)M^{2+}(OH)_2(s) + (x)M^{3+}(OH)_3(s) + (x/2)M^{2+}(A^{q-})_{(2/q)}(s)$$
$$\longleftrightarrow [M^{2+}_{1-x}M^{3+}_x(OH)_2](A^{q-})_{(x/q)}(s) \tag{64}$$

Model 3, Equation (65), is a combination of the hydroxide compounds $M^{2+}(OH)_2$, $M^{3+}(OH)_3$ with a trivalent metal-anion complex $M^{3+}_q(A^{q-})_3$ where $q = 1, 2$.

$$(1-x)M^{2+}(OH)_2(s) + (2\,x/3)\,M^{3+}(OH)_3(s) + (x/2)M^{2+}(A^{q-})_{(2/q)}(s)$$
$$\longleftrightarrow [M^{2+}_{1-x}M^{3+}_x(OH)_2](A^{q-})_{(x/q)}(s) \tag{65}$$

$\Delta_f\bar{G}°$ and $\Delta_f\bar{H}°$ for LDHs, are then able to be calculated in an additive style. Model 1, Equation (66), is presented to calculate $\Delta_f\bar{G}°$.

$$\Delta_f\bar{G}°_{LDH-M_1} = (1-x)\Delta_f\bar{G}°_{M^{2+}(OH)_2} + x\Delta_f\bar{G}°_{M^{3+}(OH)_3}$$
$$+ (x/q)\Delta_f\bar{G}°_{H_q(A^{q-})} - x\Delta_f\bar{G}°_{H_2O} \tag{66}$$

Model 4, the General Model (GM), was developed to take into account all the possible interactions of the interlayer anion and is also independent of the use of starting material. The values produced from the GM are weighted averages from the collection of single models. The model starts by looking at the LDH formula, $[M^{2+}_{1-x}M^{3+}_x(OH)_2](A^{q-})_{x/q}$, and the number of cations, NC_i, where i refers to the model number that may interact with A^{q-}.

NC_0	= 0
$NC_1(H^+)$	= 2
$NC_2(M^{2+})$	= 1 − x
$NC_3(M^{3+})$	= x
Total	= 3

The averaged value of $\Delta_f\bar{G}°$ is then calculated with the use of Equation (67).

$$\Delta_f\bar{G}°_{LDH\text{-}GM} = p_0.\Delta_f\bar{G}°_{LDH\text{-}M0} + p_1.\sum_{i=1}^{3} w_i.\Delta_f\bar{G}°_{LDH\text{-}Mi} \tag{67}$$

The quantity, p_0, is seen as the probability of having interlayer anions that do not interact with the cations in the layers of an LDH. Conversely, p_1 is the probability of having interlayer anions interacting with cations in the layers of a LDH. Therefore, $p_0 + p_1 = 1$. The weighting factor, w_i, is described by Equation (68) with I_i being an interaction parameter (bond strength) between H^+, M^{2+}, M^{3+} and A^{q-}.

$$w_i = NC_i \cdot I_i / \sum_{i=1}^{3} NC_I \cdot I_i \tag{68}$$

The models and associated thermodynamic equations were used with well-known compilations of STFP data to mainly calculate $\Delta_f\bar{G}°$ for various LDHs [68]. The modelled $\Delta_f\bar{G}°$ data can be found in Table 7.

Mechanical mixture model approaches were also applied to both Hydrothermal Reconstruction (HR) and Coprecipitation (CP) synthesis methods to investigate associated thermochemistry [69]. These models are used to calculate $\Delta_r\bar{G}°$ for LDH reactions.

HR methods, Equation (69), are similar in layout to previous mixture models described but make use of metal oxides.

$$(1-x)M^{2+}O(s) + (x/2)M^{3+}_2O(s) + (x/q)A^{q-}(aq) + (1+x/2)H_2O(l)$$
$$\longleftrightarrow [M^{2+}_{1-x}M^{3+}_x(OH)_2](A^{q-})_{(x/q)}(s) + (x)OH^-(aq) \tag{69}$$

The $\Delta_r\bar{G}°$ for a HR reaction is calculated with Equation (70).

$$\Delta_r\bar{G}°_{HR} = [\Delta_f\bar{G}°_{LDH} + (x)\Delta_f\bar{G}°_{OH^-}] - [(1-x)\Delta_f\bar{G}°_{M^{2+}O}$$
$$+ (x/2)\Delta_f\bar{G}°_{M^{3+}O} + (x/q)\Delta_f\bar{G}°_{A^{q-}} + (1+x/2)\Delta_f\bar{G}°_{H_2O}] \tag{70}$$

The synthesis can be further distinguished into 2 cases by the anion in use: hydroxyl anion $A^{q-} = OH^-$ and non-hydroxyl anion $A^{q-} \neq OH^-$.

Coprecipitation involves mixtures of metal salts, an interlayer of interest, and basic conditions to precipitate an LDH. Various combinations of metals salts and anions can be used in 5 different cases investigated.

- Case 1: divalent and trivalent metal with the same univalent anion
- Case 2: divalent and trivalent metal with the different univalent anion
- Case 3: divalent metal-univalent anion and trivalent metal-divalent anion
- Case 4: divalent metal-divalent anion and trivalent metal-univalent anion
- Case 5: divalent and trivalent metal with the same divalent anion

The reaction equation for case 1 is described by Equation (71).

$$(1-x)M^{2+}D_2^-(s) + (x/2)M_2^{3+}D_3^-(s) + 2\,OH^-(aq) + (x/q)A^{q-}(aq) \longleftrightarrow [M_{1-x}^{2+}M_x^{3+}(OH)_2](A^{q-})_{(x/q)}(s) + (2+x)D^-(aq) \quad (71)$$

With the associated $\Delta_r\bar{G}^\circ$ for CP expressed with Equation (72).

$$\begin{aligned}\Delta_r\bar{G}^\circ_{CP} =& (1-x)[\Delta_f\bar{G}^\circ_{M^{2+}(OH)_2} - \Delta_f\bar{G}^\circ_{M^{2+}(D^-)_2}] \\ &+ (x)[\Delta_f\bar{G}^\circ_{M^{3+}(OH)_3} - \Delta_f\bar{G}^\circ_{M^{3+}(D^-)_3}] \\ &+ (x)[(1/2)\Delta_f\bar{G}^\circ_{M^{2+}(A^{q-})_{2/n}} \\ &- (1/2)\Delta_f\bar{G}^\circ_{M^{2+}(OH)_2} + \Delta_f\bar{G}^\circ_{OH^-} - (1/q)\Delta_f\bar{G}^\circ_{A^{q-}}] \\ &+ (2+x)[\Delta_f\bar{G}^\circ_{D^-} - \Delta_f\bar{G}^\circ_{OH^-}] \end{aligned} \quad (72)$$

Both the HR and CP models do not fit the scope of the review for describing and obtaining STFP data as they were only intended for calculating $\Delta_r\bar{G}^\circ_{HR}$ and $\Delta_r\bar{G}^\circ_{CP}$. However, it had to be mentioned briefly as the approach is unique and with some future modification, may be used to determine STFP data. For greater detail, the referenced literature should be viewed for the full systematic explanation to calculate $\Delta_r\bar{G}^\circ_{HR}$ and $\Delta_r\bar{G}^\circ_{CP}$ for LDHs [69].

The STFP data and $\Delta_r\bar{G}^\circ$ values calculated by all these the proposed mechanical mixture models are in agreement with published experimental data on LDH solubility [68,69]. However, as evident in the model equations, the approaches ignored the effects of the associated hydration waters of an LDH (adsorbed, crystal and excess water). The comparisons made to the published experimental data are also based on solubility and redox potential studies that also ignore the hydration of LDHs [68]. The thermodynamic data produced from these models therefore only describes LDHs in a partial solid phase.

Interestingly, a short comparison study was conducted with the mixture models (model 0, 1 and 2) for $\Delta_f\bar{H}^\circ$ that factored in all the types of interlayer water. The comparison reported good agreement between the published experimental data of $[Co_{0.68}Al_{0.32}(OH)_2](CO_3)_{0.17}\cdot 0.8\,H_2O$ and $[Co_{0.76}Al_{0.24}(OH)_2](CO_3)_{0.12}\cdot 0.81\,H_2O$ and the mentioned mixture models with the same target compound compositions [29,68]. This means, with slight modification, it is possible to apply these models as full solid phase models, factoring in all types of interlayer water, and obtain the STFP data for LDHs.

Regarding interlayer water, a thermodynamic study of Allada [31] indicated that interlayer water of hydrotalcite possesses a unique state between liquid water and ice. This could potentially be applicable for all LDHs but further testing on multiple LDH variations needs to be done for confirmation. It can have a direct influence on the STFP data considered for water when factoring it into the models. A separate study conducted with mixture models on NiAl based LDH samples intercalated with carbonate (CO_3^{2-}), nitrate (NO_3^-) and sulphate (SO_4^{2-}) also revealed that interlayer water could have a potential effect on the thermodynamic data [70]. An LDH sample for each type of intercalated anion was heat-aged, causing water loss, and the extracted $\Delta_f\bar{H}^\circ$ data revealed less negative values for both the carbonate and nitrate intercalated samples. The sulphate interlayer sample was only 15 kJ mol^{-1} more negative than compared to the non-heat-aged sample. However, it is not unexpected as it has been demonstrated in a more recent study of ZnAl LDHs that SO_4^{2-} has higher hydration compared to the anions of CO_3^{2-} and CL^- in the interlayer and therefore greater stability [34]. Based on the results of the above mentioned studies, the assumption to disregard the waters associated with the LDH structure, needs to be adequately rationalised as the types of interlayer waters have a definitive effect on an LDH and the associated thermodynamic data. The assumption to disregard the waters associated with the LDH structure, therefore requires further investigation in order to rationalise the effect these types of interlayer waters have on an LDH and the associated thermodynamic models and data.

The validity of STFP data generated from the additional mechanical mixture models greatly depends on the accuracy of $\Delta_f\bar{G}^\circ$ data for each species considered [68,69]. With that statement, the majority of thermodynamic property values collected for these studies were from well-known and recognised compilations of thermochemical data, but the predicted results should still be interpreted with caution [68,69]. All the calculations involved only factored in the species considered for each reaction and therefore the model. This means STFP data produced from these models are only applicable if no other species is present, that was not considered, or when it is safe to assume that any other potential species does not have a large influencing effect on the calculated data [68,69].

The discussed models should be used as an initial guide to estimate thermodynamic properties of LDHs. If fully hydrated forms of LDHs are to be studied, the data from these models should be taken even more as a first estimate. The interlayer water has the potential to have a large effect on STFP data.

3.2.3. Solid-solution model

A solid-solution model was initially employed to describe GR LDHs with only $Fe^{2+}Fe^{3+}$ cations in the brucite-like layer, [59]. By considering Fe^{3+} ions substituting for Fe^{2+} ions within the brucite-like layers, a substitutional solid solution can be modelled as a regular solid solution model. The regular solid solution model used hypothetical end members (constituent compounds) $Fe(OH)_2$ and $Fe(OH)_3$ with a GR structure. $\Delta_f\bar{G}^\circ_{LDH}$ for $Fe^{2+}_{(1-x)}Fe^{3+}_x\,(OH)_2\cdot xOH^-$, with interlayer water omitted, is expressed by Equation (73) to Equation (75) with x indicating the extent of Fe^{3+} substitution. The model is considered a partial solid phase model for LDHs due to disregarding interlayer water.

$$\Delta_f\bar{G}^\circ_{LDH} = (1-x)\Delta_f\bar{G}^\circ_{Fe(OH)_2} + x\Delta_f\bar{G}^\circ_{Fe(OH)_3} + \Delta\bar{G}^\circ_{mix} \quad (73)$$

The standard Gibbs free energy of mixing ($\Delta\bar{G}^\circ_{mix}$) is described by Equation (74) and Equation (75) if it assumed to be a regular solid-solution.

$$\Delta\bar{G}^\circ_{mix} = \Delta\bar{G}^\circ_{mix,ideal} + \Delta\bar{G}^\circ_{excess} \quad (74)$$

$$\Delta\bar{G}^\circ_{mix} = RT[(1-x)\ln(x) + x\ln(x)] + A_0x(1-x) \quad (75)$$

The constant (A_0) was obtained by fitting $\Delta\bar{G}^\circ_{excess}$ to experimental data from previously published literature [62,71]. The assumption was made that the $Fe(OH)_2$ is similar in structure to the LDH and allows for an existing value of $\Delta_f\bar{G}^\circ_{Fe(OH)_2}$ to be used. Together with adjusting $\Delta_f\bar{G}^\circ_{Fe(OH)_3}$, Equation (73) was fitted to three experimentally determined $\Delta_f\bar{G}^\circ_{LDH}$ values from solubility methods.

A regular solid solution model was also developed for GR LDHs with $Fe^{2+}Fe^{3+}Mg^{2+}$ in the brucite-like layer (a ternary LDH) and is based of the previously described work [59,64]. It encompasses more complexity due to an extra degree of freedom from Mg component being present. However, it follows a similar scheme to construct and obtain the necessary values for the variables within the regular solid solution equation and should be reviewed for a full description [64].

Solid solution models incorporated into GEMS were used to model $\Delta_f\bar{G}^\circ_{LDH}$ data found in the *Cemdata* dataset with mainly $\Delta\bar{G}^\circ_{excess}$

Table 5
Thermochemical cycle for calculating the enthalpy of formation from carbonates and hydroxides [32,33]

$M^{2+}_{1-x}Al_x(OH)_2(CO_3)_{x/2}\cdot nH_2O(cr, 298\,K) \longrightarrow (1-3/2x)M^{2+}(OH)_2(soln, 1073\,K)$ + $x/2M^{2+}CO_3(soln, 1073\,K)$ + $xAl(OH)_3(soln, 1073\,K)$ + $nH_2O(g, 1073\,K)$	$\Delta\bar{H}_{dsol,1}$
$(1-3/2x)M^{2+}(OH)_2(cr, 298\,K) \longrightarrow (1-3/2x)M^{2+}(OH)_2(soln, 1073\,K)$	$\Delta\bar{H}_{dsol,2}$
$(x/2)M^{2+}CO_3(cr, 298\,K) \longrightarrow (x/2)M^{2+}CO_3(soln, 1073\,K)$	$\Delta\bar{H}_{dsol,3}$
$xAl(OH)_3(cr, 298\,K) \longrightarrow xAl(OH)_3(soln, 1073\,K)$	$\Delta\bar{H}_{dsol,4}$
$nH_2O(l, 298\,K) \longrightarrow nH_2O(g, 1073\,K)$	$\Delta\bar{H}_{dsol,5}$
$(1-3/2x)M^{2+}(OH)_2(cr, 298\,K)$ + $x/2M^{2+}CO_3(cr, 298\,K)$ + $xAl(OH)_3(cr, 298\,K)$ + $nH_2O(l, 298\,K) \longrightarrow M^{2+}_{1-x}Al_x(OH)_2(CO_3)_{x/2}\cdot nH_2O(cr, 298\,K)$	$\Delta_f\bar{H}_{scc}$
$\Delta_f\bar{H}_{scc} = -\Delta\bar{H}_{dsol,1} + \Delta\bar{H}_{dsol,2} + \Delta\bar{H}_{dsol,3} + \Delta\bar{H}_{dsol,4} + \Delta\bar{H}_{dsol,5}$	

Table 6
Thermochemical cycle for calculating the enthalpy of formation from oxides [32,33]

$M^{2+}_{1-x}Al_x(OH)_2(CO_3)_{x/2}\cdot nH_2O(cr, 298\,K) \longrightarrow (1-x)M^{2+}O(soln, 1073\,K)$ + $x/2Al_2O_3(soln, 1073\,K)$ + $x/2CO_2(g, 1073\,K)$ + $(1+n)H_2O(g, 1073\,K)$	$\Delta\bar{H}_{dsol,1}$
$(1-x)M^{2+}O(cr, 298\,K) \longrightarrow (1-x)M^{2+}O(soln, 1073\,K)$	$\Delta\bar{H}_{dsol,2}$
$x/2Al_2O_3(cr, 298\,K) \longrightarrow x/2Al_2O_3(soln, 1073\,K)$	$\Delta\bar{H}_{dsol,3}$
$x/2CO_2(g, 298\,K) \longrightarrow x/2CO_2(g, 1073\,K)$	$\Delta\bar{H}_{dsol,4}$
$(1+n)H_2O(l, 298\,K) \longrightarrow (1+n)(H_2O(g, 1073\,K)$	$\Delta\bar{H}_{dsol,5}$
$(1-x)M^{2+}O(cr, 298\,K)$ + $x/2Al_2O_3(cr, 298\,K)$ + $x/2CO_2(g, 298\,K)$ + $(n+1)H_2O(l, 298\,K) \longrightarrow M^{2+}_{1-x}Al_x(OH)_2(CO_3)_{x/2}\cdot nH_2O(s, 298\,K)$	$\Delta_f\bar{H}_{ox}$
$\Delta_f\bar{H}_{ox} = -\Delta\bar{H}_{dsol,1} + \Delta\bar{H}_{dsol,2} + \Delta\bar{H}_{dsol,3} + \Delta\bar{H}_{dsol,4} + \Delta\bar{H}_{dsol,5}$	

changed or modified to describe the non-ideality of the LDH solid solutions. The models available in GEMS can be viewed from the referenced literature for more insight and distinction between them [23,72–76,26,77,78].

4. Thermodynamic data measurement techniques

The methods described in this section were all utilised to experimentally determine Standard Thermodynamic Formation Property (STFP) data for Layered Double Hydroxides (LDHs). The basic implementation is described and the referenced work should be viewed if more information is desired.

4.1. High temperature oxide-melt solution calorimetry

The enthalpies of LDHs ($\Delta_f\bar{H}^\circ_{LDH}$) with interlayers containing carbonates (CO_3^{2-}) or sulphates (SO_4^{2-}) were calculated using high temperature oxide-melt solution calorimetry [79,31,34]. This was done by measuring enthalpies of drop solution ($\Delta\bar{H}_{dsol}$) for the various constituent compounds (hydroxides, carbonates, sulphates, oxides, water and LDHs) in the purpose-built Setaram AlexSYS Tian-Calvet twin microcalorimeter. The constituent compounds and LDHs are pelletised and dropped from 298 K into the calorimeter at 1073 K containing the solvent, molten sodium molybdate ($3Na_2O\cdot 4MoO_3$), in a platinum crucible [34]. The older study of Allada [31] used molten lead borate ($2PbO\cdot B_2O_3$) as solvent at 973 K. The measured $\Delta\bar{H}_{dsol}$ is a sum of the sample enthalpy content from 298 K to 1073 K and its enthalpy of solution in the solvent at 1073 K. Utilising the $\Delta\bar{H}_{dsol}$ values in thermochemical cycles, such as in Table 5 and 6, allows $\Delta_f\bar{H}_{scc}$ and $\Delta_f\bar{H}_{ox}$ to be calculated [32,33].

Finally, depending on the thermochemical cycle implemented, $\Delta_f\bar{H}^\circ_{LDH}$ is calculated from $\Delta_f\bar{H}^\circ$ data of constituent compounds obtained from literature and manipulation of Equation (7) for $\Delta_f\bar{H}_{scc}$, and Equation (8) for $\Delta_f\bar{H}_{ox}$, into Equation (77) and (76).

$$\Delta_f\bar{H}^\circ_{LDH} = \Delta_f\bar{H}_{scc} + (x/2\Delta_f\bar{H}^\circ_{MCO_3} + x\Delta_f\bar{H}^\circ_{Al(OH)_3} + (1-3/2x)\Delta_f\bar{H}^\circ_{M(OH)_2} + n\Delta_f\bar{H}^\circ_{H_2O}) \quad (76)$$

$$\Delta_f\bar{H}^\circ_{LDH} = \Delta_f\bar{H}_{ox} + ((1-x)\Delta_f\bar{H}^\circ_{MO} + x/2\Delta_f\bar{H}^\circ_{Al_2O_3} + x/2\Delta_f\bar{H}^\circ_{CO_2} + (1+n)\Delta_f\bar{H}^\circ_{H_2O}) \quad (77)$$

4.2. Low-temperature adiabatic calorimetry

Low-temperature adiabatic calorimetry also known as relaxation calorimetry is employed to obtain low-temperature $\bar{C}_p$ data. A commercially available instrument called the Physical Properties Measurement System (PPMS) produced by Quantum Design is used to conduct the analysis. It is a highly automated system that can generate acceptable third-law quality $\bar{C}_p$ data in a temperature range of 2-300 K with less than 10 mg of sample mass [39,38,37,34]. A sample is powdered, wrapped in thin Al foil and compressed to produce a 0.5 mm thick pellet which is then placed onto the sample platform of the calorimeter for measurement [38,80]. This was employed for calcium aluminate monocarbonate hydrate (hydrocalumite) with a composition of $3CaO\cdot Al_2O_3\cdot CaCO_3\cdot 10.7H_2O$ or $Ca_4Al_2(OH)_{12}CO_3\cdot 4.7H_2O$ [38]. The work by Jayanthi et al. [34] on ZnAl LDHs applies a slightly different sample preparation by encasing a sample in copper foil along with two small copper coils to enhance thermal conductivity. The sample is then pressed into a pellet and sealed in an aluminium Differential Scanning Calorimetry (DSC) pan under vacuum to prevent water loss in the PPMS.

For both preparation methods, Apiezon N grease is applied to the pellet to provide a thermal connection to the sample holder [38,34]. A correction measurement is performed before the sample measurement to account for the $\bar{C}_p$ of the sample holder and Apiezon N grease thermally linking the sample to the holder. The $\bar{C}_p$ of the copper, aluminium, and Apiezon N grease used inside the sealed DSC pans is subtracted from the measured $\bar{C}_p$ of the sample. [39,37,34].

4.3. Acid solution calorimetry

Room-temperature acid solution calorimetry was used to determine the enthalpies of formation for Mg based LDHs bearing NO_3^-, Cl^-, I^- and ReO_4^- as high-temperature oxide-melt solution calorimetry techniques are not optimised for phases containing halides and nitrates [31,34].

The same calorimetry method was applied on NiAl based LDHs bearing SO_4^{2-} and NO_3^- to retrieve $\Delta_f\bar{H}^\circ$ data on sulfate Green Rust (GR) [70,81]. More recently the method was also used on LiAl and ZnAl based LDHs containing Cl^- in the interlayer to retrieve $\Delta_f\bar{H}^\circ$ data [35,36,34]. All the referenced literature under this measurement method used the commercial, Calorimetry Science Corp (CSC) 4400 microcalorimeter, with Isothermal Microcalorimeter (IMC) software

for $\Delta_f \bar{H}°$ data retrieval. The referenced literature followed the same methodology and standards for the calorimetry method [31,70,81,35–37,34].

The enthalpy of solution ($\Delta \bar{H}_{sol}$) in HCl (Alfa Aesar, standardised) at 298 K was measured in a series 4400 IMC. This measurement indicates the heat effect associated with dropping the sample from room temperature into 5.0 N HCl at 298 K. The enthalpy of acid solution accounts for the dissolution of the solid phase, the evolution of any gases, in this case, CO_2, and the enthalpy of dilution, due to the dissolution of interlayer water into the acid. Pelletised samples were dissolved in 25 g of acid under vigorous stirring to ensure complete dissolution. The calorimeter was calibrated by dissolving 5 mg pellets of KCl (NIST standard reference material 1655) in 25 g of deionised water under the same stirring conditions [31,34].

Implementing a thermochemical cycle similar to the high temperature oxide-melt solution calorimetry method, the $\Delta \bar{H}_{sol}$ for all the constituent compounds and the LDH are measured to then eventually calculate $\Delta_f \bar{H}°_{LDH}$ [31].

4.4. Sorption balance

Sorption balance measurements were used to determine STFP data for hydrocalumite grouped LDHs [56,7]. The instrument implemented is described as the DVS Advantage (Surface Measurement Systems, London, UK). The mass of a small sample (5–100 mg) is continuously measured with an analytical balance while it is controlled by a program that varies relative humidity (RH). The desired Relative Humidity (RH) is reached by mixing different proportions of dry and water vapour saturated nitrogen (N_2) gas streams. The sorption balance enables the mass of water taken up or released during a hydration/dehydration phase transformation or deliquescence and the water activity (RH/100) at which the process takes place to be quantified. The mass is directly measured by the balance and a ramp or step program is used to determine the water activity of a specific transformation. A step program is less sensitive to disturbances and less time-consuming than a ramp program and was the regime chosen for testing of samples [56]. The constant rate of change in mass (dm/dt) sections at each RH level can be plotted as a function of the RH of the gas stream. A linear curve that intersects ($dm/dt = 0$) at the water activity indicates where an absorption/desorption process takes place [56].

4.5. Sorption calorimetry

This calorimetry technique allows for continuous scanning of water activity while simultaneously measuring water activity, moisture content and sorption enthalpy during an ad/absorption process. It is a double twin isothermal sorption calorimeter and has two measuring positions placed 90mm apart [56,7].

When the sample is introduced into the calorimeter, the thermal power of evaporation and thermal power of sorption are continuously measured by two twin microcalorimeters at the top and bottom chambers of the calorimeter.

The dry sample is loaded in the bottom chamber and water is injected into the top and is transported by diffusion to the sample during the measurement. The diffusion rate depends on the geometry of the connecting tube inside the calorimeter and the water activity over the sample. The water diffusion rate, and thus the rate of change of moisture content of the sample, is proportional to the power of evaporation. The water activity is calculated from the evaporation rate, and the mixing enthalpy, $\Delta \bar{H}_{mix}$, is calculated by comparing the thermal powers of sorption and vaporization. The enthalpy measured from the sorption microcalorimeter is normally presented as a mixing enthalpy [56,7]. It is the difference between the enthalpy of the sorption process($\Delta \bar{H}_{sorp}$) and that of condensation of liquid water ($\Delta \bar{H}_{cond}$.) The $\Delta \bar{H}_{mix}$ can be seen as an “excess enthalpy” indicating how much additional heat is obtained from a sorption process compared to condensation of water. $\Delta \bar{H}_{sorp}$, $\Delta \bar{H}_{cond}$ and the $\Delta \bar{H}_{mix}$ are related with Equation (78) and can be used to calculate $\Delta_r \bar{H}°$, Equation (79), for the hydration of a compound [56,7].

$$\Delta \bar{H}_{sorp} = \Delta \bar{H}_{cond} + \Delta \bar{H}_{mix} \tag{78}$$

$$\Delta_r \bar{H}° = \Delta \bar{H}_{sorp} \cdot n \tag{79}$$

The $\Delta \bar{H}_{sorp}$ and the $\Delta \bar{H}_{mix}$ are properties of the moisture state at which the sorption/mixing takes place, while the $\Delta \bar{H}_{cond}$ of water is constant under isothermal conditions with a value of $-44\ kJ\,mol^{-1}$ H_2O at 298 K. The thermodynamic sign convention used in this work states that processes are considered from the viewpoint of the system. This means if heat is lost by the system to the surroundings (heat is produced) the enthalpy change is negative. $\Delta \bar{H}_{sorp}$, $\Delta \bar{H}_{cond}$ and the $\Delta \bar{H}_{mix}$ are therefore all negative [56].

A separate study examined the energetics of ordered and faulted synthetic hydrotalcite used water adsorption calorimetry to evaluate the binding strength of water molecules in LDH by determining the enthalpy of water adsorption (hydration enthalpy) [8,82].

This calorimetry method uses 25 mg of LDH placed in a silica glass forked tube and is degassed at 493 K under vacuum for 5 h using the degassing port of a Micromeritics ASAP 2020 instrument. A coupled system consisting of a Micromeritics ASAP 2020 gas adsorption analyser and a Setaram Sensys Calvet microcalorimeter is then used to measure the enthalpy of adsorption of each incremental dose of water vapour. Each water dose (1 μmol) generates a distinct calorimetric peak due to heat effects associated with water adsorption, and the integral of the area under the peak provides the corresponding heat of adsorption (differential enthalpy). It is considered to be chemisorbed water until the differential enthalpy reaches the condensation enthalpy ($-44\ kJ\,mol^{-1}$) of water. Water adsorbed at $-44\ kJ\,mol^{-1}$ is considered to be physiosorbed. The reference state for water is taken to be its vapour as the associated enthalpy does not depend on pressure at constant temperature since H_2O can be considered an ideal gas at low pressures. A blank tube was also tested to correct the data for adsorbed water on the forked tube wall [8,82].

4.6. Differential Scanning Calorimetry (DSC) and Differential Thermal Analysis (DTA)

Differential Scanning Calorimetry (DSC) and Differential Thermal Analysis (DTA) methods make use of a sample’s temperature and heating and cooling measurements. Indication of heat flow corresponds to differences in temperature between a sample and a reference crucible [83]. These are well developed methods and are commonly used for biological materials, polymers, and ceramics up to 1600 °C. DTA instruments for operation up to 2400 °C are available from several manufacturers. Quantitative measurements of heat capacities and enthalpies of phase transitions from a DSC (both in the solid state and melting) are achievable when proper care is taken and appropriate calibration standards are available [84,83].

A DSC coupled with a Thermogravimetric Analysis (TGA) is used to determine the water content of LDHs such as some of the Li and Ca based LDHs found in Table 7 [7,35,36]. A power-compensated DSC was used as a supplementary technique for acid solution calorimetry to verify $\Delta_f \bar{H}°$ data near room temperature for a hydrocalumite sample also found in Table 7 [85,38].

5. Standard thermodynamic formation property data

Additional information on the Standard Thermodynamic Formation Property (STFP) data of Layered Double Hydroxides (LDHs) is provided below as a preview to Table 7.

A large portion of the data in Table 7 originates from the standard thermodynamic property tables of cement literature [26,72,53]. The references of each LDH in these tables were reviewed to identify

how the thermodynamic data were measured or estimated and can be viewed in the footnotes of Table 7.

Low-temperature adiabatic calorimetry was originally used to determine $\Delta_f \bar{H}°, \bar{S}°$ and $\Delta_f \bar{G}°$ for the LDH, $Mg_{0.74}Al_{0.26}(OH)_2(CO_3)_{0.13} \cdot 0.39H_2O$ [86,31]. The determined $\bar{S}°$ was used to validate the assumption that the entropy contribution of $T\Delta_r \bar{S}°_{scc}$ to Equation (12) is small (< 2 kJ mol^{-1}) and may be used in the calculation for $\Delta_f \bar{G}°$ for other LDHs of similar structure. The assumption was applied to various other referenced literature [30,74,72,53,24,25].

The STFP data for the hydrocalumite grouped LDHs from the Table 1 in Lothenbach et al. [26] (reported in Table 7) were obtained by employing the three-term approximation method. The exception is the investigation of the effects of Relative Humidity (RH) on the hydration states for different hydrocalumite grouped phases [7]. The STFP data for all the hydrotalcite and quintinite grouped LDHs in Table 1 of Lothenbach et al. [26] had their $\bar{S}°$ and $\bar{C}°_p$ data estimated using the additive model of Helgeson et al. [22] and using the supplementary data of $Mg_{0.74}Al_{0.26}(OH)_2(CO_3)_{0.13} \cdot 0.39H_2O$ in the model estimations [22,31]. It is suspected that all the thermodynamic values of $\Delta_f \bar{G}°$ and $\Delta_f \bar{H}°$, where it is not clear how it was acquired, employed some variation of the three-term approximation method. The three-term approximation method is integral to the modelling software, Gibbs Energy Minimisation Selektor (GEMS), used within the referenced articles and it may be a reason why the authors of the hydrotalcite and quintinite grouped LDHs did not go in-depth as to how some of the data was acquired [77,78].

The calculation of $\Delta_f \bar{S}_{scc}$ for sulphate, Green Rust (GR) LDHs of Mazeina et al. [81] (Table 7) was done by using acid solution calorimetry to determine $\Delta_f \bar{H}_{scc}$ and eventually $\Delta_f \bar{H}°$. $\Delta_f \bar{G}°$ data was gathered from the literature for the calculations. The calculations did not take into account compositional differences (Fe^{2+}/Fe^{3+} ratio, water and sulphate contents, crystallinity and disorder) between the samples from the study and the literature data [81].

The $\Delta_f \bar{G}°$ values for the other GR LDHs were obtained through redox potential and solubility measurements. It was calculated either from a series of equilibrium reactions for anhydrous GR, considering only the hydroxyl groups of the brucite-like layer, or do consider the interlayer water, based on structural considerations, therefore only the ideal amount of crystal water, that were not experimentally confirmed [61]. Solid solution models developed to estimate the $\Delta_f \bar{G}°$ for GRs also omit intercalated or adsorbed water in model calculations [59,64]. Based on the compositional and structural assumptions and a lack of reversal studies being conducted to confirm the required equilibrium conditions the values reported for GRs may be susceptible to greater uncertainty [81].

Finally, some literature reported only data in the form of $\Delta_f \bar{H}_{scc}$ and $\Delta_f \bar{H}_{ox}$ or of similar form and not as the desired STFP data and were therefore unfortunately excluded from Table 7 [8,35–37,34].

6. Conclusions

General LDH theory was broadly discussed with the focus of the review being on the thermodynamic models and STFP data available on LDHs. The different thermodynamic models presented indicate that there are various ways, some of which are very simple and some complex, to estimate STFP data for LDHs using limited initial data. The VBT and TDR methods have not yet been fully utilised to estimate data for LDHs and are promising methods to be used in the future.

In most of the modelling methods, caution is advised for implementation as consideration towards assumptions on the models needs to be taken seriously to prevent error in calculation. This is especially important for the considered structures of constituent compounds and in the inclusion or exclusion of interlayer water.

It is also evident from the reported literature that there is a large collection of STFP data available on LDHs, but a large portion is modelled with limited or no experimental verification. The majority of the STFP values are determined through a modelling method combined with a solubility or redox potential method with very few using calorimetry methods. $\Delta_f \bar{H}°$ data on many different LDHs have been reported but only three have near complete sets of STFP data, missing only $\bar{V}$, that have been produced through calorimetry. The data of $Mg_{0.74}Al_{0.26}(OH)_2(CO_3)_{0.13} \cdot 0.39H_2O$ was used to determine the STFP data for many other LDHs with the use of assumptions and modelling methods reported. The LDHs, $Ca_4Al_2(OH)_{12}(CO_3)_3 \cdot 4.7H_2O$ and $Mg_{0.72}Al_{0.22}Zr_{0.025}(OH)_2(Cl)_{0.20} \cdot 0.69H_2O$, both missing $\bar{V}$, are the only other two nearly completely described LDHs with no other full sets of STFP found that were determined through calorimetry.

It would be good practice to produce more full sets of STFP data through calorimetry methods and to validate the data produced through modelling methods or other measurement techniques. The technology to determine STFP data for LDHs is available with multiple methods existing and should be used to expand it.

Nomenclature

Thermochemical quantities

$\bar{C}_p$	heat capacity at constant pressure (J mol^{-1} K^{-1})
$\bar{C}°_p$	standard heat capacity at constant pressure (J mol^{-1} K^{-1})
$\bar{C}°_V$	standard heat capacity at constant volume (J mol^{-1} K^{-1})
$\Delta_r \bar{C}°_p$	standard heat capacity of reaction (J mol^{-1} K^{-1})
$\bar{H}$	molar enthalpy (kJ mol^{-1})
$\bar{S}$	molar entropy (J mol^{-1} K^{-1})
$\bar{G}$	molar Gibbs energy (kJ mol^{-1})
$\bar{V}$	molar volume (m^3 mol^{-1})
$\Delta_f \bar{H}°$	standard enthalpy of formation at 298 K (kJ mol^{-1})
$\bar{S}°$	standard absolute entropy at 298 K (J mol^{-1} K^{-1})
$\Delta_f \bar{G}°$	standard gibbs energy of formation at 298 K (kJ mol^{-1})
$\bar{V}°$	standard molar Volume at 298 K (cm^3 mol^{-1})
$\Delta \bar{G}°_{mix}$	standard gibbs energy of mixing (kJ mol^{-1})
$\Delta \bar{G}°_{mix,ideal}$	standard gibbs energy of mixing (kJ mol^{-1})
$\Delta \bar{G}°_{excess}$	standard gibbs energy of mixing (kJ mol^{-1})
$\Delta_f \bar{H}_{scc}$	enthalpy of formation for single-cation hydroxides and carbonates, and water (kJ mol^{-1})
$\Delta_f \bar{S}_{scc}$	entropy of formation for single-cation hydroxides and carbonates, and water (kJ mol^{-1})
$\Delta_f \bar{G}_{scc}$	Gibbs energy of formation for single-cation hydroxides and carbonates, and water (kJ mol^{-1})
$\Delta_f \bar{H}_{ox}$	enthalpy of formation from oxides (kJ mol^{-1})
$\Delta \bar{H}_{dsol}$	enthalpy of drop solution (kJ mol^{-1})
$\Delta \bar{H}_{sol}$	enthalpy of solution (kJ mol^{-1})
$\Delta_r \bar{H}°$	standard enthalpy of reaction at 298 K (kJ mol^{-1})
$\Delta_r \bar{S}°$	standard entropy of reaction at 298 K (J mol^{-1} K^{-1})
$\Delta_r \bar{G}°$	standard Gibbs energy of reaction at 298K (kJ mol^{-1})
$\Delta_r \bar{V}°$	standard volume of reaction at 298 K (cm^3 mol^{-1})
E	electrochemical potential (V)
$E°$	standard electrochemical potential (V)
Q	reaction quotient
$\Delta \bar{H}_{sorp}$	enthalpy of sorption (kJ mol^{-1})
$\Delta \bar{H}_{cond}$	enthalpy of condensation (kJ mol^{-1})
$\Delta \bar{H}_{mix}$	enthalpy of mixing (kJ mol^{-1})
f	equilibrium fugacity of compound
f^*	fugacity of a pure compound at T
RH	equilibrium relative humidity
a_w	water activity

Constituent thermochemical quantities

$\bar{S}°_j$	standard molar entropy of the inorganic compound of interest, j (J mol^{-1} K^{-1})

Table 7
Thermodynamic data and estimates on LDHs.

LDH	$\Delta_f \bar{G}°$ (kJ mol^{-1})	$\Delta_f \bar{H}°$ (kJ mol^{-1})	$\bar{S}°$ (J mol^{-1} K^{-1})	a_o[1] (J mol^{-1} K^{-1})	a_1[1] (J K^{-2} mol^{-1})	a_2[1] (J K mol^{-1})	a_3[1] (J K$^{-0.5}$ mol^{-1})	$\bar{V}°$ (cm^3 mol^{-1})	Ref
Hydrocalumite Group									
$Ca_4Al_2(OH)_{14} \cdot 12H_2O$[a]	–8749.9	–10017.9	1120	1163	1.047		–1600	369	[57]
$Ca_4Al_2(OH)_{14} \cdot 6H_2O$[b]	–7325.7	–8262.4	831.5	208.3	3.13			274	[7]
$Ca_4Al_2(OH)_{14} \cdot 6H_2O$[a]	–7326.6	–8302	700	711	1.047		–1600	274	[23]
$Ca_4Al_2(OH)_{14} \cdot 4H_2O$[b]	–6841.4	–7656.6	772.7	0.0119	3.56	1.341×10^{-7}		257	[7]
$Ca_2Al_2(OH)_{10} \cdot 2.5H_2O$[a]	–4695.5	–5277.5	450	323	0.728			180	[57]
$Ca_2Al_2(OH)_{10} \cdot 3H_2O$[a]	–4812.8	–5433	440	392	0.714		–800	184	[25], [23]
$CaAl_2(OH)_8 \cdot 6H_2O$[a]	–4623.0	–5288.2	610	151	1.113		3200	193	[57]
$Ca_4Al_2(OH)_{13}(CO_3)_{0.5} \cdot 5.5H_2O$[a]	–7335.97	–8270	713	664	1.014	-1.301×10^6	–800	285	[25], [23]
$Ca_4Al_2(OH)_{13}(CO_3)_{0.5} \cdot 4H_2O$[b]	–6970.3	–7813.3	668.3	0.0095	2.836	1.071×10^{-7}		261	[7]
$Ca_4Al_2(OH)_{13}(CO_3)_{0.5} \cdot 2.5H_2O$[b]	–6597.4	–7349.7	622.5	0.0088	2.635	9.941×10^{-8}		249	[7]
$Ca_4Al_2(OH)_{12}CO_3 \cdot 5H_2O$[a]	–7337.46	–8250	657	618	0.982	-2.591×10^6		262	[25], [23]
$Ca_4Al_2(OH)_{12}CO_3 \cdot 4.7H_2O$[c]	–7272.0±8.7	–8166.6±7.7	652.4 ± 2.2						[38]
$Ca_4Al_2(OH)_{12}CO_3 \cdot 3H_2O$[b]	–6840.3	–7618.6	640.6	192.4	2.042			234	[7][b]
$Ca_4Al_2(OH)_{12}SO_4 \cdot 10H_2O$[b]	–8726.8	–9930.5	975.0	636	1.606			351	[7]
$Ca_4Al_2(OH)_{12}SO_4 \cdot 8H_2O$[b]	–8252.9	–9321.8	960.9	1028.5				332	[7]
$Ca_4Al_2(OH)_{12}SO_4 \cdot 6H_2O$[b]	–7778.4	–8758.6	791.6	175	2.594			310	[7]
$Ca_4Al_2(OH)_{12}SO_4 \cdot 6H_2O$[a]	–7778.5	–8750	821	594	1.168			309	[23]
$Ca_4Al_2(OH)_{12}SO_4 \cdot 4.5H_2O$[b]	–7414.9	–8311.9	721	172	2.402			282	[7]
$Ca_4Al_2(OH)_{12}SO_4 \cdot 3H_2O$[b]	7047.6	–7845.5	703.6	169	2.211			275	[7]
$Ca_2Al_2(OH)_{10}SiO_2 \cdot 3H_2O$[a]	–5705.15	–6360	546	438	0.749	-1.131×10^6	–800	216	[25], [23]
$Ca_2Al_2(OH)_{10}SiO_2 \cdot 2H_2O$[b]	–5464.0	–6066.8	487.6	0.0063	1.887	7.121×10^{-8}		215	[7]
$Ca_2Al_2(OH)_{10}SiO_2 \cdot 0.5H_2O$[b]	–5095.2	–5603.4	454.8	0.0057	1.685	6.361×10^{-8}		213	[7]
$Ca_4Al_2(OH)_{12}Cl(SO_4)_{0.5} \cdot 6H_2O$[a]	–7533.4	–8472	820	557	1.141	-1.021×10^6	751	289	[87]
$Ca_4Al_2(OH)_{12}Cl_2 \cdot 4H_2O$[a]	–6814.6	–7625	731	498	0.89	-2.031×10^6	1503	272	[87]
$Ca_4Al_2(OH)_{12}(NO_3)_2 \cdot 4H_2O$[a]	–6778.1	–7719.3	821	580	1.02	-2.771×10^6	872	296	[88]
$Ca_4Al_2(OH)_{12}(NO_2)_2 \cdot 4H_2O$[a]	–6606.8	–7493.1	799	565	0.99	-2.241×10^6	703	275	[88]
$Ca_4Fe_2(OH)_{14} \cdot 6H_2O$[a]	–6438.6	–7434.9	630	694	1.113	2.021×10^6	1600	286	[89]
$Ca_4Fe_2(OH)_{13}(CO_3)_{0.5} \cdot 3.5H_2O$[a]	–5952.9	–6581	1270	308	1.201	-9.081×10^5	3200	273	[90]
$Ca_4Fe_2(OH)_{12}CO_3 \cdot 6H_2O$[a]	–6674.0	–7485	1230	612	1.157	-5.731×10^5		292	[90]
$Ca_4Fe_2(OH)_{12}SO_4 \cdot 6H_2O$[a]	–6873.2	–7663	1430	577	1.234	2.021×10^6		321	[91]
$Ca_4Fe_2(OH)_{12}Cl_2 \cdot 4H_2O$[a]	–5900.1	–6528	1286	481	0.961	-1.611×10^4	1503	278	[91]
Fougèrite Group									
$Fe^{2+}_{0.57}Fe^{3+}_{0.43}(OH)_{1.72}(SO_4)_{0.36} \cdot 0.91H_2O$		–1079.6 ±1.6[e]							[81]
$Fe^{2+}_{0.55}Fe^{3+}_{0.45}(OH)_{1.70}(SO_4)_{0.38} \cdot 0.90H_2O$		–1084.4 ±1.6[e]							[81]
$Fe^{2+}_{0.47}Fe^{3+}_{0.53}(OH)_{1.85}(SO_4)_{0.34} \cdot 0.82H_2O$		–1068.6 ±2.2[e]							[81]
$Fe^{2+}_{0.33}Fe^{3+}_{0.67}(OH)_{2.01}(SO_4)_{0.33} \cdot 0.59H_2O$		–1036.8 ±1.5[e]							[81]
$Fe^{2+}_6Fe^{3+}_2(OH)_{16}(C_2O_4) \cdot 3H_2O$	–5383 ±3[f]								[65]

Table 7 (*continued*)

LDH	$\Delta_f\bar{G}°$ (kJ mol^{-1})	$\Delta_f\bar{H}°$ (kJ mol^{-1})	$\bar{S}°$ (J mol^{-1} K^{-1})	a_o[l] (J mol^{-1} K^{-1})	a_1[l] (J K^{-2} mol^{-1})	a_2[l] (J K mol^{-1})	a_3[l] (J K$^{-0.5}$ mol^{-1})	$\bar{V}°$ (cm^3 mol^{-1})	Ref
Fougèrite Group									
$Fe^{2+}_4Fe^{3+}_2(OH)_{12}(SO_4)\cdot nH_2O$	–3790 ±10[f]								[66]
$Fe^{2+}_4Fe^{3+}_2(OH)_{12}(SO_4)\cdot 3H_2O$	–4380 ±4[f]								[55]
$Fe^{2+}_6Fe^{3+}_2(OH)_{16}(SO_3)\cdot 4H_2O$	–5465 ±14[f]								[67]
$Fe^{2+}_3Fe^{3+}(OH)_8(Cl)\cdot nH_2O$	–2145 ±7[f]								[92]
$Fe^{2+}_4Fe^{3+}_2(OH)_{12}(CO_3)\cdot 2H_2O$	–4042.79 ±0[f]								[60]
$Fe_{0.67}Fe_{0.33}(OH)_2(SO_4)_{0.17}$ (Model 0)	–632.5								[68]
$Fe_{0.67}Fe_{0.33}(OH)_2(SO_4)_{0.17}$ (Model 1)	–606.0								[68]
$Fe_{0.67}Fe_{0.33}(OH)_2(SO_4)_{0.17}$ (Model 2)	–616.6								[68]
$Fe_{0.67}Fe_{0.33}(OH)_2(SO_4)_{0.17}$ (Model 3)	–630.5								[68]
$Fe_{0.67}Fe_{0.33}(OH)_2(SO_4)_{0.17}$ (GM)	–621.8								[68]
$Fe_{0.75}Fe_{0.25}(OH)_2(Cl)_{0.25}$ (Model 0)	–535.2								[68]
$Fe_{0.75}Fe_{0.25}(OH)_2(Cl)_{0.25}$ (Model 1)	–515.2								[68]
$Fe_{0.75}Fe_{0.25}(OH)_2(Cl)_{0.25}$ (Model 2)	–519.2								[68]
$Fe_{0.75}Fe_{0.25}(OH)_2(Cl)_{0.25}$ (Model 3)	–510.2								[68]
$Fe_{0.75}Fe_{0.25}(OH)_2(Cl)_{0.25}$ (GM)	–525.5								[68]
$Fe_{0.67}Fe_{0.33}(OH)_2(CO_3)_{0.17}$ (Model 0)	–596.5								[68]
$Fe_{0.67}Fe_{0.33}(OH)_2(CO_3)_{0.17}$ (Model 1)	–585.7								[68]
$Fe_{0.67}Fe_{0.33}(OH)_2(CO_3)_{0.17}$ (Model 2)	–592.6								[68]
Hydrotalcite Group									
$Mg_{0.74}Al_{0.26}(OH)_2(CO_3)_{0.13}\cdot 0.39H_2O$	–1043.08 ± 2.07	–1165.98 ± 2.06[d]	85.58 ± 0.17[g]						[31]
$Mg_{0.73}Al_{0.27}(OH)_2(CO_3)_{0.16}\cdot 0.83H_2O$		–1297.19 ± 1.97[d]							[32]
$Mg_{0.74}Al_{0.26}[(NO_3)_{0.2}(OH)_{0.06}](OH)_2\cdot 0.39H_2O$		–1119.36 ± 2.50[e]							[32]
$Mg_{0.74}Al_{0.26}[I_{0.23}(OH)_{0.03}](OH)_2\cdot 0.39H_2O$		–1079.32 ± 2.32[e]							[32]
$Mg_{0.74}Al_{0.26}[(ReO_4)_{0.17}(OH)_{0.09}](OH)_2\cdot 0.40H_2O$		–1181.82 ± 2.26[e]							[32]
$Mg_{0.73}Al_{0.27}[Cl_{0.22}(OH)_{0.05}](OH)_2\cdot 0.83H_2O$		–1252.34 ± 2.12[e]							[32]
$Mg_6Al_2(OH)_{18}\cdot 3H_2O$	–8022.9[a]	–9006.7[a]	675.2[h]	803.1[h]				305.4	[72]
$Mg_3Al(OH)_8(CO_3)_{0.5}\cdot 2.5H_2O$	–4339.85[f]	–4875.89[a]	411.46[h]	512.60[h]				115	[74]
$Mg_3Fe(OH)_8(CO_3)_{0.5}\cdot 2.5H_2O$	–3882.6[f]	–4415.09[a]	422.51[j]	521.27[j]				119	[74]
$Mg_{0.75}Al_{0.25}(OH)_2(Cl)_{0.25}$ (Model 0)	–907.9								[68]
$Mg_{0.75}Al_{0.25}(OH)_2(Cl)_{0.25}$ (Model 1)	–887.8								[68]
$Mg_{0.75}Al_{0.25}(OH)_2(Cl)_{0.25}$ (Model 2)	–884.2								[68]
$Mg_{0.75}Al_{0.25}(OH)_2(Cl)_{0.25}$ (Model 3)	–879.5								[68]
$Mg_{0.75}Al_{0.25}(OH)_2(Cl)_{0.25}$ (GM)	–897.1								[68]
$Mg_{0.75}Al_{0.25}(OH)_2(NO_3)_{0.25}$ (Model 0)	–902.9								[68]
$Mg_{0.75}Al_{0.25}(OH)_2(NO_3)_{0.25}$ (Model 1)	–882.9								[68]
$Mg_{0.75}Al_{0.25}(OH)_2(NO_3)_{0.25}$ (Model 2)	–883.8								[68]
$Mg_{0.75}Al_{0.25}(OH)_2(NO_3)_{0.25}$ (Model 3)	–882.9								[68]
$Mg_{0.75}Al_{0.25}(OH)_2(NO_3)_{0.25}$ (GM)	–893.0								[68]

(*continued on next page*)

Table 7 (*continued*)

LDH	$\Delta_f\tilde{G}°$ (kJ mol^{-1})	$\Delta_f\tilde{H}°$ (kJ mol^{-1})	$\tilde{S}°$ (J mol^{-1} K^{-1})	a_o[l] (J mol^{-1} K^{-1})	a_1[l] (J K^{-2} mol^{-1})	a_2[l] (J K mol^{-1})	a_3[l] (J K$^{-0.5}$ mol^{-1})	$\tilde{V}°$ (cm^3 mol^{-1})	Ref
Hydrotalcite Group									
$Ni_{0.77}Al_{0.23}(OH)_2(CO_3)_{0.12}\cdot 0.33\,H_2O$		–838.18 ± 1.26[d]							[33]
$Ni_{0.75}Al_{0.25}(OH)_2(Cl)_{0.25}$ (Model 0)	–614.1								[68]
$Ni_{0.75}Al_{0.25}(OH)_2(Cl)_{0.25}$ (Model 1)	–594.0								[68]
$Ni_{0.75}Al_{0.25}(OH)_2(Cl)_{0.25}$ (Model 2)	–597.8								[68]
$Ni_{0.75}Al_{0.25}(OH)_2(Cl)_{0.25}$ (Model 3)	–585.7								[68]
$Ni_{0.75}Al_{0.25}(OH)_2(Cl)_{0.25}$ (GM)	–604.2								[68]
$Ni_{0.75}Al_{0.25}(OH)_2(NO_3)_{0.25}$ (Model 0)	–609.1								[68]
$Ni_{0.75}Al_{0.25}(OH)_2(NO_3)_{0.25}$ (Model 1)	–589.1								[68]
$Ni_{0.75}Al_{0.25}(OH)_2(NO_3)_{0.25}$ (Model 2)	–594.9								[68]
$Ni_{0.75}Al_{0.25}(OH)_2(NO_3)_{0.25}$ (Model 3)	–589.1								[68]
$Ni_{0.75}Al_{0.25}(OH)_2(NO_3)_{0.25}$ (GM)	–599.8								[68]
$Zn_{0.75}Al_{0.25}(OH)_2(Cl)_{0.25}$ (Model 0)	–698.6								[68]
$Zn_{0.75}Al_{0.25}(OH)_2(Cl)_{0.25}$ (Model 1)	–678.5								[68]
$Zn_{0.75}Al_{0.25}(OH)_2(Cl)_{0.25}$ (Model 2)	–682.2								[68]
$Zn_{0.75}Al_{0.25}(OH)_2(Cl)_{0.25}$ (Model 3)	–670.1								[68]
$Zn_{0.75}Al_{0.25}(OH)_2(Cl)_{0.25}$ (GM)	–688.7								[68]
$Zn_{0.75}Al_{0.25}(OH)_2(NO_3)_{0.25}$ (Model 0)	–693.6								[68]
$Zn_{0.75}Al_{0.25}(OH)_2(NO_3)_{0.25}$ (Model 1)	–673.6								[68]
$Zn_{0.75}Al_{0.25}(OH)_2(NO_3)_{0.25}$ (Model 2)	–673.1								[68]
$Zn_{0.75}Al_{0.25}(OH)_2(NO_3)_{0.25}$ (Model 3)	–673.6								[68]
$Zn_{0.75}Al_{0.25}(OH)_2(NO_3)_{0.25}$ (GM)	–683.5								[68]
Quintinite Group									
$Mg_4Al_2(OH)_{14}\cdot 3\,H_2O$	–6394.56[f]	–7196[a]	549[h]	–364[h]	4.21[h]	3.75e6[h]	629[hi]	220	[24] [25]
$Mg_4Al_2(OH)_{12}CO_3\cdot 2\,H_2O$	–6580.15[f]	–7374[a]	551[h]	–382[h]	4.24[h]	4.32e6[h]	629[hi]	220	[24], [25]
$Mg_4Al_2(OH)_{14}\cdot 3\,H_2O$	–6358.5[a]	–7160.2[a]	548.9[h]	547.6[h]				219.1	[72]
$Mg_{0.67}Al_{0.33}(OH)_2(CO_3)_{0.16}\cdot 0.70\,H_2O$		–1284.65 ± 1.75[d]							[31]
$Mg_{0.66}Al_{0.34}(OH)_2(CO_3)_{0.17}\cdot 0.69\,H_2O$		–1292.07 ± 1.63[d]							[31]
$Mg_{0.69}Al_{0.31}(OH)_2(CO_3)_{0.15}\cdot 0.30\,H_2O$		–1168.52 ± 1.8[d]							[54]
$Mg_4Al_2(OH)_{14}\cdot 3\,H_2O$	–6407.21[k]	–7219.64[k]	552.07[h]	556.15[h]				227.36	[53]
$Mg_4Al_2(OH)_{12}CO_3\cdot 2\,H_2O$	–6295.37[k]	–7078.83[k]	512.96[h]	604.15[h]				231.46	[53]
$Zn_{0.67}Al_{0.33}(OH)_2(CO_3)_{0.17}\cdot 0.30\,H_2O$		–993.04 ± 0.96[d]							[54]
$Zn_{0.66}Al_{0.33}(OH)_2(Cl)_{0.333}\cdot 0.560\,H_2O$			111.30 ± 2.22						[34]
$Zn_{0.66}Al_{0.33}(OH)_2(CO_3)_{0.167}\cdot 0.389\,H_2O$			102.80 ± 2.06						[34]
$Zn_{0.66}Al_{0.33}(OH)_2(SO_4)_{0.144}(CO_3)_{0.023}\cdot 0.731\,H_2O$			126.68 ± 2.34						[34]

Table 7 (*continued*)

LDH	$\Delta_f\bar{G}°$ (kJ mol^{-1})	$\Delta_f\bar{H}°$ (kJ mol^{-1})	$\bar{S}°$ (J mol^{-1} K^{-1})	a_o[l] (J mol^{-1} K^{-1})	a_1[l] (J K^{-2} mol^{-1})	a_2[l] (J K mol^{-1})	a_3[l] (J K$^{-0.5}$ mol^{-1})	$\bar{V}°$ (cm^3 mol^{-1})	Ref
Glaucocerinite Group									
$Ni_{0.66}Al_{0.34}(OH)_2[(SO_4)_{0.15}(CO_3)_{0.02}]\cdot 0.21\,H_2O$		–940.30 ± 1.64[e]							[70]
$Ni_{0.65}Al_{0.35}(OH)_2[(SO_4)_{0.15}(CO_3)_{0.02}]\cdot 0.22\,H_2O$		–957.52 ± 1.89[e]							[70]
$Ni_{0.72}Al_{0.28}(OH)_2[(SO_4)_{0.12}(CO_3)_{0.02}]\cdot 0.43\,H_2O$		–952.78 ± 1.71[e]							[70]
Ungrouped									
$Co_{0.68}Al_{0.32}(OH)_2(CO_3)_{0.16}\cdot 0.78\,H_2O$		–1044.17 ± 2.54[d]							[29]
$Co_{0.69}Al_{0.31}(OH)_2(CO_3)_{0.16}\cdot 0.68\,H_2O$		–1006.26 ± 1.62[d]							[33]
$Co_{0.70}Al_{0.30}(OH)_2(CO_3)_{0.16}\cdot 0.23\,H_2O$		–877.34 ± 1.35[d]							[54]
$Co_{0.76}Al_{0.24}(OH)_2(CO_3)_{0.12}\cdot 0.81\,H_2O$		–991.79 ±1.72[d]							[29]
$Co_{0.80}Al_{0.20}(OH)_2(CO_3)_{0.10}\cdot 0.76\,H_2O$		–933.36 ± 2.17[d]							[33]
$Co_{0.83}Al_{0.17}(OH)_2(CO_3)_{0.09}\cdot 0.29\,H_2O$		–777.09 ± 1.97[d]							[33]
$Co_{0.756}Al_{0.244}(OH)_2[(CO_3)_{0.1202}(NO_3)_{0.0018}]\cdot 0.810\,H_2O$		–967.89 ± 3.33[d]							[29]
$Co_{0.68}Al_{0.32}(OH)_2(CO_3)_{0.17}\cdot 0.80\,H_2O$ (Model 0)		–1041.7							[68]
$Co_{0.68}Al_{0.32}(OH)_2(CO_3)_{0.17}\cdot 0.80\,H_2O$ (Model 1)		–1027.4							[68]
$Co_{0.68}Al_{0.32}(OH)_2(CO_3)_{0.17}\cdot 0.80\,H_2O$ (Model 2)		–1039.1							[68]
$Co_{0.76}Al_{0.24}(OH)_2(CO_3)_{0.12}\cdot 0.81\,H_2O$ (Model 0)		–984.0							[68]
$Co_{0.76}Al_{0.24}(OH)_2(CO_3)_{0.12}\cdot 0.81\,H_2O$ (Model 1)		–973.1							[68]
$Co_{0.76}Al_{0.24}(OH)_2(CO_3)_{0.12}\cdot 0.81\,H_2O$ (Model 2)		–982.0							[68]
$LiAl_2(OH)_6Cl\cdot 3.20\,H_2O$			288.37 ± 5.38						[37]
$Li_{1.03}Al_2(OH)_6Cl_{1.03}\cdot 2.47\,H_2O$			262.51 ± 4.90						[37]
$Li_{0.73}Al_2(OH)_6Cl_{0.73}\cdot 2.06\,H_2O$			275.86± 5.03						[37]
$Li_{0.57}Al_{1.56}Fe_{0.44}(OH)_6Cl_{0.57}\cdot 1.11\,H_2O$			233.31 ± 3.86						[37]
$Li_{0.78}Al_{1.77}Fe_{0.23}(OH)_6Cl_{0.78}\cdot 0.96\,H_2O$			220.74 ± 3.67						[37]
$Mg_{0.72}Al_{0.22}Zr_{0.025}(OH)_2(Cl)_{0.20}\cdot 0.69\,H_2O$	–1046 ± 7	–1181 ± 5[e]	97 ± 7	102					[39]
$Mg_{0.72}Al_{0.22}Zr_{0.025}(OH)_2(Cl)_{0.20}\cdot 0.69\,H_2O$ (GEM Model)	–1046 ± 13								[39]
$Mg_8Al_2(OH)_{22}\cdot 3\,H_2O$	–9687.4[a]	–10853.3[a]	801.5[h]	957.7[h]				392.4	[72]
$Ni_{0.65}Al_{0.35}(OH)_2[(NO_3)_{0.21}(CO_3)_{0.07}]\cdot 0.42\,H_2O$		–942.41 ± 2.07[e]							[70]
$Ni_{0.66}Al_{0.34}(OH)_2[(NO_3)_{0.24}(CO_3)_{0.05}]\cdot 0.30\,H_2O$		–904.03 ± 1.94[e]							[70]
$Ni_{0.77}Al_{0.23}(OH)_2[(NO_3)_{0.13}(CO_3)_{0.05}]\cdot 0.60\,H_2O$		–908.42 ± 2.02[e]							[70]
$Ni_{0.65}Al_{0.35}(OH)_2[(CO_3)_{0.02}(H_3SiO_4)_{0.15}]\cdot 0.08\,H_2O$		–1132.27 ± 1.37[d]							[70]
$Ni_{0.69}Al_{0.31}(OH)_2(CO_3)_{0.16}\cdot 0.37\,H_2O$		–918.42 ± 1.21[d]							[54]
$Ni_{0.66}Al_{0.34}(OH)_2(CO_3)_{0.17}\cdot 0.42\,H_2O$		–904.031 ± 0.93[d]							[33]
$Ni_{0.67}Al_{0.33}(OH)_2(CO_3)_{0.17}\cdot 0.41\,H_2O$		–908.42 ± 2.06[d]							[33]
$Ni_{0.64}Al_{0.36}(OH)_2(CO_3)_{0.18}\cdot 0.46\,H_2O$		–942.41 ± 1.53[d]							[33]

[a] Data modelled with three–term approximation method (GEMS or similar software) and solubility data.
[b] Calculated from $\Delta_r G°, \Delta_r H°, \Delta_r S°$ of hydration states and from referenced data of [23] and [57].
[c] Data determined with acid–solution calorimetry and relaxation calorimetry.
[d] Determined with high–temperature oxide melt solution calorimetry.
[e] Determined with acid–solution calorimetry.
[f] Determined with solubility or redox potential measurements.
[g] Determined with adiabatic calorimetry.
[h] Helgeson's method using thermodynamic data of hydrotalcite from [22,31].
[i] $\bar{C}_p° = a_0 + a_1T + a_2T^{-2} + a_3T^{-0.5} - 0.00424\,T^2 + 2.11\,e{\mp}6\,T^3$.
[j] Estimated by assuming same reaction changes of S and Cp of hydrotalcite applies to pyroaurite due to lack of calorimetry data [74].
[k] Acquisition of thermodynamic value not clearly specified, though highly probable three-term approximation method.
[l] $\bar{C}_p° = a_0 + a_1T + a_2T^{-2} + a_3T^{-0.5}$.

$\bar{S}_i^\circ$ standard molar entropy of the constituent oxide or hydroxide i^{th} species ($J\,mol^{-1}\,K^{-1}$)
$\bar{S}_{\hat{i}}^\circ$ standard molar entropy of i^{th} species of interest ($J\,mol^{-1}\,K^{-1}$)
$\bar{V}_i$ molar volume of constituent species, i ($m^3\,mol^{-1}$)
$\bar{V}_j$ molar volume of constituent species of interest, j ($m^3\,mol^{-1}$)
S_{vib} vibrational entropy ($J\,mol^{-1}\,K^{-1}$)
S_{config} configurational entropy ($J\,mol^{-1}\,K^{-1}$)
$S_{config,brucite}$ configurational entropy of brucite layer ($J\,mol^{-1}\,K^{-1}$)
$S_{config,interlayer}$ configurational entropy of interlayer ($J\,mol^{-1}\,K^{-1}$)

Thermochemical quantity set

P thermochemical quantity set: $\Delta_f\bar{G}^\circ$, $\Delta_f\bar{H}^\circ$, $\bar{S}^\circ$, V_N, or U_{POT}

Chemical formulae

M cation element
M^+ monovalent cation
M^{2+} divalent cation
M^{3+} trivalent cation
M^{4+} quadrivalent cation
A interlayer anion or anion element
A^{q-} interlayer anion with charge
B interlayer cation or cation
C polytype symbol
D general non-intercalated anion in solution
q charge

Compositional quantities

n amount of interlayer water or hydration water mol
ν_i stoichiometric coefficient of species in compound
$n_{modelled}$ modelled water content mol
$\hat{\nu}_{i,r}$ stoichiometric coefficient of species in reaction
$\hat{\nu}_{\hat{i},r}$ stoichiometric coefficient of species of interest in reaction
n_{Va} vacant interlayer sites
n_t total moles of mixing species mol
b stoichiometric amount of cation mol
a stoichiometric amount of anion mol
x cation mole fraction
x_a interlayer anion mole fraction
x_w water content mole fraction
x_{Va} mole fraction of vacant sites
y mole amount M^{2+}
z mole amount M^{3+}

Non-compositional potentials

T temperature (K)
p pressure (kPa)

Crystallographic quantities

V_{cell} unit cell volume ($Å^3$)
V_N formula unit volume ($nm^3 \cdot formula-unit^{-1}$)
N formula unit
N_{anion} number of formula unit (anion) sites occupied by anions
NC_i number of cations that may interact with A
N_A Avogadro's number ($N_A = 6.022 \times 10^{23}\ formula-unit \cdot mol^{-1}$)
U_{POT} lattice potential energy ($kJ\,mol^{-1}$)
I_i interaction parameter

Statistical Thermochemical Properties

p_0 probability of interlayer anions not interacting with the cations
p_1 probability of interlayer anions interacting with the cations
w_i weighting factor

TDR Method Property Constants

$\theta_P(H_2O, s\text{-}s)$ thermodynamic property constant for H_2O ($kJ\,mol^{-1}(H_2O\,molecule)^{-1}$)
$\theta_{V_N}(H_2O, s\text{-}s)$ formula unit volume constant for H_2O ($nm^3(H_2O\,molecule)^{-1}$)
$\theta_{\Delta_f\bar{H}^\circ}(H_2O, s\text{-}s)$ standard enthalpy of formation constant for H_2O ($kJ\,mol^{-1}(H_2O\,molecule)^{-1}$)
$\theta_{\bar{S}^\circ}(H_2O, s\text{-}s)$ standard absolute entropy constant for H_2O ($J\,mol^{-1}\,K^{-1}(H_2O\,molecule)^{-1}$)
$\theta_{\Delta_f\bar{G}^\circ}(H_2O, s\text{-}s)$ standard gibbs energy of formation for H_2O constant ($kJ\,mol^{-1}(H_2O\,molecule)^{-1}$)
$\theta_{U_{POT}}(H_2O, s\text{-}s)$ lattice potential energy constant for H_2O ($kJ\,mol^{-1}(H_2O\,molecule)^{-1}$)
$\theta_P(SOL, s\text{-}s)$ thermodynamic property constant for solvate ($kJ\,mol^{-1}(SOL\,molecule)^{-1}$)
$\theta_{\Delta_f\bar{H}^\circ}(SOL, s\text{-}s)$ standard enthalpy of formation constant for solvate ($kJ\,mol^{-1}(SOL\,molecule)^{-1}$)
$\theta_{\bar{S}^\circ}(SOL, s\text{-}s)$ standard absolute entropy constant for solvate ($J\,mol^{-1}\,K^{-1}(SOL\,molecule)^{-1}$)
$\theta_{\Delta_f\bar{G}^\circ}(SOL, s\text{-}s)$ standard gibbs energy of formation constant for solvate ($kJ\,mol^{-1}(SOL\,molecule)^{-1}$)
$\theta_{U_{POT}}(SOL, s\text{-}s)$ lattice potential energy constant for solvate ($kJ\,mol^{-1}(SOL\,molecule)^{-1}$)

Extended Debye-Huckel Parameters

a activity
a_w water activity
γ_i activity coefficient of ion i
A Debye-Hűckel solvent parameter, dependent on the dielectric constant of water and temperature
B Debye-Hűckel solvent parameters, dependent on the dielectric constant of water and temperature
z ionic charge
z_i ionic charge of ion i
α_i size of ion-dependent parameter
b semi-empirical parameter ($b = 0.064$ at 298 K)
I effective ionic strength
K_{sp} solubility product constant at specific temperature
K_f fugacity equilibrium constant

Empirical Constants

k' constant, the value depends on the constituent type and coordination state ($k' \approx 1\ J\,mol^{-1}\,K^{-1}(nm^3 \cdot formula-unit)$ at 298 K)
k empirically determined constant ($J\,mol^{-1}\,K^{-1}$)
c empirically determined constant ($J\,mol^{-1}\,K^{-1}$)
R universal gas constant ($R = 8.314\ J\,mol^{-1}\,K^{-1}$)
F Faraday constant ($F = 96.5\ kJ\,mol^{-1}$)
A_0 regular solid solution constant ($kJ\,mol^{-1}$)
a_0 heat capacity coefficient ($J\,mol^{-1}\,K^{-1}$)
a_1 heat capacity coefficient ($J\,mol^{-1}\,K^{-2}$)
a_2 heat capacity coefficient ($J\,K\,mol^{-1}$)
a_3 heat capacity coefficient ($J\,mol^{-1}\,K^{-0.5}$)

Acronyms

CNMNC Commission on New Minerals, Nomenclature and Classification
CP Coprecipitation

CSC	Calorimetry Science Corp
CSP	Complete Solid Phase
DSC	Differential Scanning Calorimetry
DTA	Differential Thermal Analysis
DVS	Dynamic Vapour Sorption
GEMS	Gibbs Energy Minimisation Selektor
GM	General Model
GR	Green Rust
HR	Hydrothermal Reconstruction
IMC	Isothermal Microcalorimeter
IUPAC	International Union of Pure and Applied Chemistry
LDH	Layered Double Hydroxide
LDHs	Layered Double Hydroxides
PPMS	Physical Properties Measurement System
PSP	Partial Solid Phase
RH	Relative Humidity
SI	International System of Units
STFP	Standard Thermodynamic Formation Property
STRP	Standard Thermodynamic Reaction Property
TDR	Thermodynamic Difference Rules
TGA	Thermogravimetric Analysis
VBT	Volume-Based Thermodynamics
XRD	X-Ray Diffraction

Declaration of competing interest

The authors declare that they have no known competing financial interests or personal relationships that could have appeared to influence the work reported in this paper.

Data availability

Data will be made available on request.

References

[1] C. Forano, T. Hibino, F. Leroux, C. Taviot-Guého, Chapter 13.1 Layered Double Hydroxides, Developments in Clay Science, vol. 1, Elsevier, 2006, pp. 1021–1095, https://linkinghub.elsevier.com/retrieve/pii/S1572435205010391.

[2] S. Naseem, B. Gevers, F.J.W.J. Labuschagné, A. Leuteritz, Catalytic degradation study of iron (Fe) containing LDH-PP composites, Mallorca, Spain, 2020, p. 020041, http://aip.scitation.org/doi/abs/10.1063/5.0028406.

[3] L. Tabana, S. Tichapondwa, F. Labuschagne, E. Chirwa, Adsorption of phenol from wastewater using calcined magnesium-zinc-aluminium layered double hydroxide clay, Sustainability 12 (2020) 4273, https://doi.org/10.3390/su12104273, https://www.mdpi.com/2071-1050/12/10/4273.

[4] S. Naseem, B.R. Gevers, F.J.W.J. Labuschagné, A. Leuteritz, Preparation of Photoactive Transition-Metal Layered Double Hydroxides (LDH) to Replace Dye-Sensitized Materials in Solar Cells, Materials 13 (2020) 4384, https://doi.org/10.3390/ma13194384, https://www.mdpi.com/1996-1944/13/19/4384, vol. number: 19, Publisher: Multidisciplinary Digital Publishing Institute.

[5] S.J. Mills, A.G. Christy, J.-M.R. Génin, T. Kameda, F. Colombo, Nomenclature of the hydrotalcite supergroup: natural layered double hydroxides, Mineral. Mag. 76 (2012) 1289–1336, https://doi.org/10.1180/minmag.2012.076.5.10, https://www.cambridge.org/core/journals/mineralogical-magazine/article/abs/nomenclature-of-the-hydrotalcite-supergroup-natural-layered-double-hydroxides/5719A401C83C37F3ED7A11205A57DC84.

[6] S. Marappa, P. Kamath, Water molecules in hydrotalcite-like layered double hydroxides: interplay between the hydration of the anions and the metal hydroxide layer: water molecules in hydrotalcite-like layered double hydroxides, ZAAC 641 (5) (2015) 927–934, https://doi.org/10.1002/zaac.201500065.

[7] L.G. Baquerizo, T. Matschei, K.L. Scrivener, M. Saeidpour, L. Wadsö, Hydration states of AFm cement phases, Cem. Concr. Res. 73 (2015) 143–157, https://doi.org/10.1016/j.cemconres.2015.02.011, https://linkinghub.elsevier.com/retrieve/pii/S0008884615000538.

[8] R. Shivaramaiah, A. Navrotsky, Energetics of order-disorder in layered magnesium aluminum double hydroxides with interlayer carbonate, Inorg. Chem. 54 (2015) 3253–3259, https://doi.org/10.1021/ic502820q, https://pubs.acs.org/doi/10.1021/ic502820q.

[9] B.R. Gevers, E. Roduner, F.J.W.J. Labuschagné, Towards understanding photon absorption and emission in MgAl layered double hydroxide, Mater Adv. 3 (2022) 962–977, https://doi.org/10.1039/D1MA00893E, http://xlink.rsc.org/?DOI=D1MA00893E.

[10] S.M. Auerbach, K.A. Carrado, P.K. Dutta (Eds.), Handbook of Layered Materials, M. Dekker, New York, 2004, OCLC: ocm55063501.

[11] B.R. Gevers, S. Naseem, A. Leuteritz, F.J.W.J. Labuschagné, Comparison of nanostructured transition metal modified tri-metal MgMAl–LDHs (M = Fe, Zn, Cu, Ni, Co) prepared using co-precipitation, RSC Adv. 9 (2019) 28262–28275, https://doi.org/10.1039/C9RA05452A, http://xlink.rsc.org/?DOI=C9RA05452A.

[12] F. Cavani, F. Trifirò, A. Vaccari, Hydrotalcite-type anionic clays: preparation, properties and applications, Catal. Today 11 (1991) 173–301, https://doi.org/10.1016/0920-5861(91)80068-K, https://www.sciencedirect.com/science/article/pii/092058619180068K.

[13] F.J.W.J. Labuschagné, A. Wiid, H.P. Venter, B.R. Gevers, A. Leuteritz, Green synthesis of hydrotalcite from untreated magnesium oxide and aluminum hydroxide, Green Chem. Lett. Rev. 11 (2018) 18–28, https://doi.org/10.1080/17518253.2018.1426791, https://www.tandfonline.com/doi/full/10.1080/17518253.2018.1426791.

[14] B.R. Gevers, Green Synthesis of Hydrocalumite (CaAl-OH-LDH) from Ca(OH)2 and Al(OH)3 and the Parameters That Influence Its Formation and Speciation, 2020, p. 26.

[15] S. Aisawa, N. Higashiyama, S. Takahashi, H. Hirahara, D. Ikematsu, H. Kondo, H. Nakayama, E. Narita, Intercalation behavior of l-ascorbic acid into layered double hydroxides, Appl. Clay Sci. 35 (2007) 146–154, https://doi.org/10.1016/j.clay.2006.09.003, https://linkinghub.elsevier.com/retrieve/pii/S0169131706001700.

[16] J.A. Dyer, N.C. Scrivner, S.K. Dentel, A practical guide for determining the solubility of metal hydroxides and oxides in water, Environ. Prog. 17 (1998) 1–8, https://doi.org/10.1002/ep.670170112, http://onlinelibrary.wiley.com/doi/abs/10.1002/ep.670170112, https://onlinelibrary.wiley.com/doi/pdf/10.1002/ep.670170112.

[17] M.R. Othman, Z. Helwani Martunus, W.J.N. Fernando, Synthetic hydrotalcites from different routes and their application as catalysts and gas adsorbents: a review, Appl. Organomet. Chem. 23 (2009) 335–346, https://doi.org/10.1002/aoc.1517, http://onlinelibrary.wiley.com/doi/abs/10.1002/aoc.1517, https://onlinelibrary.wiley.com/doi/pdf/10.1002/aoc.1517.

[18] H.P. Venter, Optimisation of the synthesis of Mg-Al-CO3 LDH and the partial substitution of Mg/Ca-based LDHs, Ph.D. thesis, 2013.

[19] M.J. Schmidt, Synthesis of Modified Hydrocalumite: a Novel Katoite/Portlandite Precursor Method, Dissertation, University of Pretoria, 2016, https://repository.up.ac.za/handle/2263/53103, accepted: 2016-06-14T07:30:32Z.

[20] S.J. Mills, F. Hatert, E.H. Nickel, G. Ferraris, The standardisation of mineral group hierarchies: application to recent nomenclature proposals, Eur. J. Mineral. (2009) 1073–1080, https://doi.org/10.1127/0935-1221/2009/0021-1994, publisher: Schweizerbart'sche Verlagsbuchhandlung.

[21] V. Gold (Ed.), The IUPAC Compendium of Chemical Terminology: The Gold Book, 4 ed., International Union of Pure and Applied Chemistry (IUPAC), Triangle Park, NC, 2019, https://goldbook.iupac.org/.

[22] H. Helgeson, J.M. Delany, H. Nesbitt, D. Bird, Summary and critique of the thermodynamic properties of rock forming minerals, undefined, https://www.semanticscholar.org/paper/Summary-and-critique-of-the-thermodynamic-of-rock-Helgeson-Delany/b9397545926d4c923660f6a30604247347b6fd3a, 1978.

[23] T. Matschei, B. Lothenbach, F.P. Glasser, Thermodynamic properties of Portland cement hydrates in the system CaO-Al2O3-SiO2-CaSO4-CaCO3-H2O, Cem. Concr. Res. 37 (2007) 1379–1410, https://doi.org/10.1016/j.cemconres.2007.06.002, https://linkinghub.elsevier.com/retrieve/pii/S0008884607001299.

[24] B. Lothenbach, F. Winnefeld, Thermodynamic modelling of the hydration of Portland cement, Cem. Concr. Res. 36 (2006) 209–226, https://doi.org/10.1016/j.cemconres.2005.03.001, https://linkinghub.elsevier.com/retrieve/pii/S000888460500075X.

[25] B. Lothenbach, T. Matschei, G. Möschner, F.P. Glasser, Thermodynamic modelling of the effect of temperature on the hydration and porosity of Portland cement, Cem. Concr. Res. 38 (2008) 1–18, https://doi.org/10.1016/j.cemconres.2007.08.017, https://linkinghub.elsevier.com/retrieve/pii/S0008884607001998.

[26] B. Lothenbach, D.A. Kulik, T. Matschei, M. Balonis, L. Baquerizo, B. Dilnesa, G.D. Miron, R.J. Myers, Cemdata18: a chemical thermodynamic database for hydrated Portland cements and alkali-activated materials, Cem. Concr. Res. 115 (2019) 472–506, https://doi.org/10.1016/j.cemconres.2018.04.018, https://linkinghub.elsevier.com/retrieve/pii/S0008884617312073.

[27] W.S. Fyfe, J. Verhoogen, F.J. Turner, Geological Society of America, Metamorphic Reactions and Metamorphic Facies, Geological Society of America, New York, 1958, OCLC: 523229.

[28] S. Ghazizadeh, T. Hanein, J.L. Provis, T. Matschei, Estimation of standard molar entropy of cement hydrates and clinker minerals, Cem. Concr. Res. 136 (2020) 106188, https://doi.org/10.1016/j.cemconres.2020.106188, https://linkinghub.elsevier.com/retrieve/pii/S0008884620304701.

[29] R.k. Allada, Thermochemistry and aqueous solubilities of hydrotalcite-like solids, Science 296 (2002) 721–723, https://doi.org/10.1126/science.1069797, https://www.sciencemag.org/lookup/doi/10.1126/science.1069797.

[30] R.K. Allada, Thermochemistry of hydrotalcite-like compounds relevant to the fate and transport of aqueous and anionic species in the environment, Ph.D. thesis, 2004, http://books.google.com/books?id=ui60dZFig1QC.

[31] R.k. Allada, Thermochemistry of hydrotalcite-like phases in the MgO-Al2O3-CO2-H2O system: a determination of enthalpy, entropy, and free energy, Am. Mineral. 90 (2005) 329–335, https://doi.org/10.2138/am.2005.1737, https://pubs.geoscienceworld.org/ammin/article/90/2-3/329-335/44370.

[32] R.K. Allada, J.D. Pless, T.M. Nenoff, A. Navrotsky, Thermochemistry of hydrotalcite-like phases intercalated with CO_3^{2-}, NO_3^-, Cl^-, i^-, and ReO_4^-, Chem. Mater. 17 (2005) 2455–2459, https://doi.org/10.1021/cm047813x, https://pubs.acs.org/doi/10.1021/cm047813x.

[33] R.K. Allada, E. Peltier, A. Navrotsky, W.H. Casey, C.A. Johnson, H.T. Berbeco, D.L. Sparks, Calorimetric determination of the enthalpies of formation OF hydrotalcite-like solids and their use in the geochemical modeling of metals in natural waters, Clays Clay Miner. 54 (2006) 9.

[34] K. Jayanthi, G. Neilsen, A. Gibson, A. Navrotsky, B.F. Woodfield, Role of anions in stabilizing the [Zn–Al] layered double hydroxides: a thermodynamic Study, J. Phys. Chem. 127 (2023) 3760–3768, https://doi.org/10.1021/acs.jpcc.2c08217.

[35] L. Wu, L. Li, S.F. Evans, T.A. Eskander, B.A. Moyer, Z. Hu, P.J. Antonick, S. Harrison, M.P. Paranthaman, R. Riman, A. Navrotsky, Lithium aluminum-layered double hydroxide chlorides (LDH): Formation enthalpies and energetics for lithium ion capture, J. Am. Ceram. Soc. (2018) jace.16150, https://doi.org/10.1111/jace.16150, https://onlinelibrary.wiley.com/doi/abs/10.1111/jace.16150.

[36] L. Wu, S. Evans, Y. Cheng, A. Navrotsky, B. Moyer, S. Harrison, P. Paranthaman, Neutron spectroscopic and thermochemical characterization of lithium–aluminum layered double hydroxide chloride: implications for lithium, Recovery 123 (2019), https://doi.org/10.1021/acs.jpcc.9b04340.

[37] Jayanthi Kumar, G. Neilsen, P. Rosen, C. Andersen, M. Dickson, S. Evan, M. Paranthaman, A. Navrotsky, B. Woodfield, Cryogenic heat capacity measurements and thermodynamic analysis of lithium aluminum layered double hydroxides (LDHs) with intercalated chloride, Am. Mineral. 107 (2022) 709–715, https://doi.org/10.2138/am-2021-7935.

[38] F. Bellmann, J. Majzlan, K.-D. Grevel, E. Dachs, H.-M. Ludwig, Analysis of thermodynamic data of calcium aluminate monocarbonate hydrate, Cem. Concr. Res. 116 (2019) 89–94, https://doi.org/10.1016/j.cemconres.2018.10.012, https://linkinghub.elsevier.com/retrieve/pii/S0008884618308597.

[39] J. Poonoosamy, F. Brandt, M. Stekiel, P. Kegler, M. Klinkenberg, B. Winkler, V. Vinograd, D. Bosbach, G. Deissmann, Zr-containing layered double hydroxides: synthesis, characterization, and evaluation of thermodynamic properties, Appl. Clay Sci. 151 (2018) 54–65, https://doi.org/10.1016/j.clay.2017.10.013, https://www.sciencedirect.com/science/article/pii/S0169131717304519.

[40] L. Ingram, The crystal structures of Sjögrenite and pyroaurite, Mineral. Mag. 36 (1967) 465–479, https://doi.org/10.1180/minmag.1967.036.280.01, http://adsabs.harvard.edu/abs/1967MinM...36..465I.

[41] L. Glasser, H.D.B. Jenkins, Predictive thermodynamics for ionic solids and liquids, Phys. Chem. Chem. Phys. 18 (2016) 21226–21240, https://doi.org/10.1039/C6CP00235H, http://xlink.rsc.org/?DOI=C6CP00235H.

[42] L. Glasser, Thermodynamics of condensed phases: formula unit volume, V_m, and the determination of the number of formula units, Z, in a crystallographic unit cell, J. Chem. Educ. 88 (2011) 581–585, https://doi.org/10.1021/ed900046k, https://pubs.acs.org/doi/abs/10.1021/ed900046k.

[43] L. Glasser, Volume-Based Thermoelasticity: Compressibility of Mineral-Structured Materials, 2010, https://pubs.acs.org/doi/pdf/10.1021/jp101512f, archive Location: world Publisher: American Chemical Society.

[44] L. Glasser, Volume-Based Thermoelasticity: Compressibility of Inorganic Solids, 2010, https://pubs.acs.org/doi/pdf/10.1021/ic902475n, archive Location: world Publisher: American Chemical Society.

[45] U. Preiss, C. Jungnickel, J. Thöming, I. Krossing, J. Łuczak, M. Diedenhofen, A. Klamt, Predicting the critical micelle concentrations of aqueous solutions of ionic liquids and other ionic surfactants, Chem. Eur. J. 15 (2009) 8880–8885, https://doi.org/10.1002/chem.200900024, https://onlinelibrary.wiley.com/doi/abs/10.1002/chem.200900024, https://onlinelibrary.wiley.com/doi/pdf/10.1002/chem.200900024.

[46] U.P.R.M. Preiss, J.M. Slattery, I. Krossing, In silico prediction of molecular volumes, heat capacities, and temperature-dependent densities of ionic liquids, Ind. Eng. Chem. Res. 48 (2009) 2290–2296, https://doi.org/10.1021/ie801268a, https://pubs.acs.org/doi/10.1021/ie801268a.

[47] H.D.B. Jenkins, L. Glasser, Standard absolute entropy, values from volume or density. 1. Inorganic Materials, Inorg. Chem. 42 (2003) 8702–8708, https://doi.org/10.1021/ic030219p, https://pubs.acs.org/doi/10.1021/ic030219p.

[48] L. Glasser, H.B. Jenkins, Standard absolute entropies, S°298, from volume or density, Thermochim. Acta 414 (2004) 125–130, https://doi.org/10.1016/j.tca.2003.12.006, https://linkinghub.elsevier.com/retrieve/pii/S004060310300683X.

[49] H.D.B. Jenkins, L. Glasser, Difference Rule A New Thermodynamic Principle: Prediction of Standard Thermodynamic Data for Inorganic Solvates, Journal of the American Chemical Society, vol. 126, American Chemical Society, Publisher, 2004, pp. 15809–15817.

[50] L. Glasser, H.D.B. Jenkins, Predictive thermodynamics for condensed phases, Chem. Soc. Rev. 34 (2005) 866, https://doi.org/10.1039/b501741f, http://xlink.rsc.org/?DOI=b501741f.

[51] H.D.B. Jenkins, L. Glasser, Thermodynamic difference rules: a prescription for their application and usage to approximate thermodynamic data†, J. Chem. Eng. Data 55 (2010) 4231–4238, https://doi.org/10.1021/je100383t, https://pubs.acs.org/doi/10.1021/je100383t.

[52] L. Glasser, H.D.B. Jenkins, Volume-based thermodynamics: a prescription for its application and usage in approximation and prediction of thermodynamic data, J. Chem. Eng. Data 56 (2011) 874–880, https://doi.org/10.1021/je100683u, https://pubs.acs.org/doi/10.1021/je100683u.

[53] P. Blanc, X. Bourbon, A. Lassin, E. Gaucher, Chemical model for cement-based materials: thermodynamic data assessment for phases other than C-S-H, Cem. Concr. Res. 40 (2010) 1360–1374, https://doi.org/10.1016/j.cemconres.2010.04.003, https://linkinghub.elsevier.com/retrieve/pii/S0008884610001031.

[54] C.A. Johnson, F.P. Glasser, Hydrotalcite-like minerals (M2Al(OH)6(CO3)0.5.XH2O, where M = Mg, Zn, Co, Ni) in the environment: synthesis, characterization and thermodynamic stability, Clays Clay Miner. 51 (2003) 1–8, https://doi.org/10.1346/CCMN.2003.510101.

[55] H.C.B. Hansen, O.K. Borggaard, J. Sl, Evaluation of the free energy of formation of Fe(H)-Fe(II1) hydroxide-su~phate (green rust) and its reduction of nitrite, 1994, p. 10.

[56] L.G. Baquerizo, T. Matschei, K.L. Scrivener, M. Saeidpour, A. Thorell, L. Wadsö, Methods to determine hydration states of minerals and cement hydrates, Cem. Concr. Res. 65 (2014) 85–95, https://doi.org/10.1016/j.cemconres.2014.07.009, https://linkinghub.elsevier.com/retrieve/pii/S0008884614001495.

[57] B. Lothenbach, L. Pelletier-Chaignat, F. Winnefeld, Stability in the system CaO-Al2O3-H2O, Cem. Concr. Res. 42 (2012) 1621–1634, https://doi.org/10.1016/j.cemconres.2012.09.002, https://linkinghub.elsevier.com/retrieve/pii/S0008884612001949.

[58] V. Rives, Layered Double Hydroxides: Present and Future, Nova Science Publishers, Huntington, N.Y., 2001, OCLC: 48046007.

[59] J.-M.R. Génin, P. Refait, G. Bourrié, M. Abdelmoula, F. Trolard, Structure and stability of the Fe(II)-Fe(III) green rust “fougerite” mineral and its potential for reducing pollutants in soil solutions, Appl. Geochem. 16 (2001) 559–570, https://doi.org/10.1016/S0883-2927(00)00043-3, https://linkinghub.elsevier.com/retrieve/pii/S0883292700000433.

[60] S.H. Drissi, P. Refait, M. Abdelmoula, J.M.R. Génin, The preparation and thermodynamic properties of Fe(II)Fe(III), hydroxide-carbonate (green rust 1); Pourbaix Diagram of Iron in Carbonate-Containing Aqueous Media, Corros. Sci. 37 (1995) 2025–2041, https://doi.org/10.1016/0010-938X(95)00096-3, https://www.sciencedirect.com/science/article/pii/0010938X95000963.

[61] H.F.W. Taylor, Crystal Structures of Some Double Hydroxide Minerals, Mineral. Mag. 39 (1973) 377–389, https://doi.org/10.1180/minmag.1973.039.304.01, publisher: Cambridge University Press, https://www.cambridge.org/core/journals/mineralogical-magazine/article/abs/crystal-structures-of-some-double-hydroxide-minerals/7A66C1808683E81970A9F578A8A376D2.

[62] J.-M.R. Génin, G. Bourrié, F. Trolard, M. Abdelmoula, A. Jaffrezic, P. Refait, V. Maitre, B. Humbert, A. Herbillon, Thermodynamic Equilibria in Aqueous Suspensions of Synthetic and Natural Fe(II)-Fe(III) Green Rusts: Occurrences of the Mineral in Hydromorphic Soils, Environ. Sci. Technol. 32 (1998) 1058–1068, https://doi.org/10.1021/es970547m, publisher: American Chemical Society.

[63] J.W. Boclair, P.S. Braterman, Layered double hydroxide stability. 1. Relative stabilities of layered double hydroxides and their simple counterparts, Chem. Mater. 11 (1999) 298–302, https://doi.org/10.1021/cm980523u, https://pubs.acs.org/doi/10.1021/cm980523u.

[64] G. Boorrié, F. Trolard, P. Refait, F. Feder, A solid-solution model for Fe(II)-Fe(III)-Mg(II) green rusts and fougerite and estimation of their Gibbs free energies of formation, Clays Clay Miner. 52 (2004) 382–394, https://doi.org/10.1346/CCMN.2004.0520313.

[65] P. Refait, A. Charton, J.-M. Génin, Identification, composition, thermodynamic and structural properties of a pyroaurite-like iron(II)-iron (III) hydroxy-oxalate green rust, Eur. J. Solid State Inorg. Chem. 35 (1998) 655–666, https://doi.org/10.1016/S0992-4361(99)80006-X, https://linkinghub.elsevier.com/retrieve/pii/S099243619980006X.

[66] P. Refait, C. Bon, L. Simon, G. Bourrié, F. Trolard, J. BessiÃre, J.-M.R. GÃnin, Chemical composition and Gibbs standard free energy of formation of Fe(II)-Fe(III) hydroxysulphate green rust and Fe(II) hydroxide, Clay Miner. 34 (1999) 499–510, https://doi.org/10.1180/000985599546280, https://www.cambridge.org/core/journals/clay-minerals/article/abs/chemical-composition-and-gibbs-standard-free-energy-of-formation-of-feiifeiii-hydroxysulphate-green-rust-and-feii-hydroxide/2BA0D9AE308EABC483778C0D576F2F93.

[67] L. Simon, J.M.R. Génin, P. Refait, Standard free enthalpy of formation of Fe(II)-Fe(III) hydroxysulphite green rust one and its oxidation into hydroxysulphate green rust two, Corros. Sci. 39 (1997) 1673–1685, https://doi.org/10.1016/S0010-938X(97)00074-7, https://www.sciencedirect.com/science/article/pii/S0010938X97000747.

[68] J.J. Bravo-Suárez, E.A. Páez-Mozo, S.T. Oyama, Models for the estimation of thermodynamic properties of layered double hydroxides: application to the study of their anion exchange characteristics, Quim Nova 27 (2004) 574–581, https://doi.org/10.1590/S0100-40422004000400011, https://www.scielo.br/j/qn/a/FwzrvHpHVKQCqXL5bwfzmFm/?lang=en.

[69] J.J. Bravo-Suárez, E.A. Páez-Mozo, S.T. Oyama, Review of the synthesis of layered double hydroxides: a thermodynamic approach, Quim Nova 27 (2004) 601–614, https://doi.org/10.1590/S0100-40422004000400015, https://www.scielo.br/j/qn/a/Pyc3LgRQ33BJbfWs7wc7Zgw/.

[70] E. Peltier, R. Allada, A. Navrotsky, D.L. Sparks, Nickel solubility and precipitation in soils: a thermodynamic study, Clays Clay Miner. 54 (2006) 153–164, https://doi.org/10.1346/CCMN.2006.0540202.

[71] G. Bourrié, F. Trolard, J.-M.R.G. Jaffrezic, V. Maître, M. Abdelmoula, Iron control by equilibria between hydroxy-green rusts and solutions in hydromorphic soils, Geochim. Cosmochim. Acta 63 (1999) 3417–3427, https://doi.org/10.1016/S0016-7037(99)00262-8, https://linkinghub.elsevier.com/retrieve/pii/S0016703799002628.

[72] R.J. Myers, B. Lothenbach, S.A. Bernal, J.L. Provis, Thermodynamic modelling of alkali-activated slag cements, Appl. Geochem. 61 (2015) 233–247, https://doi.org/10.1016/j.apgeochem.2015.06.006, https://linkinghub.elsevier.com/retrieve/pii/S0883292715001511.

[73] K. Rozov, U. Berner, C. Taviot-Gueho, F. Leroux, G. Renaudin, D. Kulik, L. Diamond, Synthesis and characterization of the LDH hydrotalcite–pyroaurite solid-solution series, Cem. Concr. Res. 40 (8) (2010) 1248–1254, https://doi.org/10.1016/j.cemconres.2009.08.031, https://linkinghub.elsevier.com/retrieve/pii/S0008884609002506.

[74] K.B. Rozov, U. Berner, D.A. Kulik, L.W. Diamond, Solubility and thermodynamic properties of carbonate-bearing hydrotalcite–pyroaurite solid solutions with a 3:1 Mg/(Al+Fe) mole ratio, Clays Clay Miner. 59 (2011) 215–232, https://doi.org/10.1346/CCMN.2011.0590301, http://link.springer.com/10.1346/CCMN.2011.0590301.

[75] K. Rozov, H. Curtius, A. Neumann, D. Bosbach, Synthesis, characterization and stability properties of Cl-bearing hydrotalcite-pyroaurite solids, Radiochim. Acta 101 (2013) 101–109, https://doi.org/10.1524/ract.2013.2007.

[76] K. Rozov, H. Curtius, D. Bosbach, Preparation, characterization and thermodynamic properties of Zr-containing Cl-bearing layered double hydroxides (LDHs), Radiochim. Acta 103 (5) (2015) 369–378, https://doi.org/10.1515/ract-2014-2326.

[77] D.A. Kulik, T. Wagner, S.V. Dmytrieva, G. Kosakowski, F.F. Hingerl, K.V. Chudnenko, U.R. Berner, GEM-selektor geochemical modeling package: revised algorithm and GEMS3K numerical kernel for coupled simulation codes, Comput. Geosci. (2012), https://doi.org/10.1007/s10596-012-9310-6, http://link.springer.com/10.1007/s10596-012-9310-6.

[78] T. Wagner, D.A. Kulik, F.F. Hingerl, S.V. Dmytrieva, GEM-Selektor Geochemical Modeling Package: TSolMod Library and Data Interface for Multicomponent Phase Models, Can. Mineral. 50 (2012) 1173–1195, https://doi.org/10.3749/canmin.50.5.1173, http://www.canmin.org/cgi/doi/10.3749/canmin.50.5.1173.

[79] A. Navrotsky, Progress and new directions in high temperature calorimetry revisited, Phys. Chem. Miner. 24 (1997) 222–241, https://doi.org/10.1007/s002690050035, http://link.springer.com/10.1007/s002690050035.

[80] C.A. Geiger, E. Dachs, Recent developments and the future of low- T calorimetric investigations in the Earth sciences: consequences for thermodynamic calculations and databases, J. Metamorph. Geol. 36 (2018) 283–295, https://doi.org/10.1111/jmg.12291, https://onlinelibrary.wiley.com/doi/10.1111/jmg.12291.

[81] L. Mazeina, A. Navrotsky, D. Dyar, Enthalpy of formation of sulfate green rusts, Geochim. Cosmochim. Acta 72 (2008) 1143–1153, https://doi.org/10.1016/j.gca.2007.11.032, https://linkinghub.elsevier.com/retrieve/pii/S0016703707006928.

[82] S.V. Ushakov, A. Navrotsky, Direct measurements of water adsorption enthalpy on hafnia and zirconia, Appl. Phys. Lett. 87 (2005) 164103, https://doi.org/10.1063/1.2108113, http://aip.scitation.org/doi/10.1063/1.2108113.

[83] S. Sarge, G. Höhne, W. Hemminger, Calorimetry: Fundamentals, Instrumentation and Applications, 2014, p. 280.

[84] A. Navrotsky, New developments in the calorimetry of high-temperature materials, Engineering 5 (2019) 366–371, https://doi.org/10.1016/j.eng.2019.03.003, https://linkinghub.elsevier.com/retrieve/pii/S2095809918307367.

[85] A. Benisek, H. Kroll, E. Dachs, The heat capacity of fayalite at high temperatures, Am. Mineral. 97 (2012) 657–660, https://doi.org/10.2138/am.2012.3924.

[86] R. Stevens, J. Boerio-Goates, Heat capacity of copper on the ITS-90 temperature scale using adiabatic calorimetry, J. Chem. Thermodyn. 36 (2004) 857–863, https://doi.org/10.1016/j.jct.2004.06.008, https://linkinghub.elsevier.com/retrieve/pii/S0021961404001223.

[87] M. Balonis, B. Lothenbach, G. Le Saout, F.P. Glasser, Impact of chloride on the mineralogy of hydrated Portland cement systems, Cem. Concr. Res. 40 (2010) 1009–1022, https://doi.org/10.1016/j.cemconres.2010.03.002, https://linkinghub.elsevier.com/retrieve/pii/S000888461000058X.

[88] M. Balonis, M. Mędala, F.P. Glasser, Influence of calcium nitrate and nitrite on the constitution of AFm and AFt cement hydrates, Adv. Cem. Res. 23 (2011) 129–143, https://doi.org/10.1680/adcr.10.00002, http://www.icevirtuallibrary.com/doi/10.1680/adcr.10.00002.

[89] B.Z. Dilnesa, B. Lothenbach, G. Renaudin, A. Wichser, D. Kulik, Synthesis and characterization of hydrogarnet Ca3(AlxFe1-x)2(SiO4)y(OH)4(3-y), Cem. Concr. Res. 59 (2014) 96–111, https://doi.org/10.1016/j.cemconres.2014.02.001, https://linkinghub.elsevier.com/retrieve/pii/S000888461400043X.

[90] B. Dilnesa, B. Lothenbach, G. Le Saout, G. Renaudin, A. Mesbah, Y. Filinchuk, A. Wichser, E. Wieland, Iron in carbonate containing AFm phases, Cem. Concr. Res. 41 (2011) 311–323, https://doi.org/10.1016/j.cemconres.2010.11.017, https://linkinghub.elsevier.com/retrieve/pii/S0008884610002607.

[91] B.Z. Dilnesa, B. Lothenbach, G. Renaudin, A. Wichser, E. Wieland, Stability of monosulfate in the presence of iron, J. Am. Ceram. Soc. 95 (2012) 3305–3316, https://doi.org/10.1111/j.1551-2916.2012.05335.x, https://onlinelibrary.wiley.com/doi/10.1111/j.1551-2916.2012.05335.x.

[92] P. Refait, J.-M. Génin, The oxidation of ferrous hydroxide in chloride-containing aqueous media and pourbaix diagrams of green rust one, Corros. Sci. 34 (1993) 797–819, https://doi.org/10.1016/0010-938X(93)90101-L, https://linkinghub.elsevier.com/retrieve/pii/0010938X9390101L.